

Pharmacokinetic Optimization of Class-Selective Histone Deacetylase Inhibitors and Identification of Associated Candidate Predictive Biomarkers of Hepatocellular Carcinoma Tumor Response

Jason C. Wong,^{*,†,‡,§} Guozhi Tang,[†] Xihan Wu,[†] Chungeng Liang,[†] Zhenshan Zhang,[†] Lei Guo,[†] Zhengong Peng,[†] Weixing Zhang,[†] Xianfeng Lin,[†] Zhanguo Wang,[†] Jianghua Mei,[†] Junli Chen,[†] Song Pan,[†] Nan Zhang,[†] Yongfu Liu,[†] Mingwei Zhou,[†] Lichun Feng,[†] Weili Zhao,[†] Shijie Li,[†] Chao Zhang,[†] Meifang Zhang,[†] Yiping Rong,[†] Tai-Guang Jin,[†] Xiongwen Zhang,[†] Shuang Ren,[†] Ying Ji,[†] Rong Zhao,[†] Jin She,[†] Yi Ren,[†] Chunping Xu,[‡] Dawei Chen,[‡] Jie Cai,[‡] Song Shan,[§] Desi Pan,[§] Zhiqiang Ning,[§] Xianping Lu,[§] Taiping Chen,[‡] Yun He,[†] and Li Chen[†]

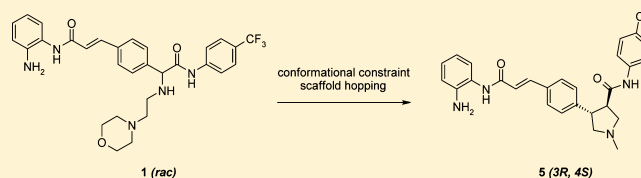
[†]Roche R&D Center (China) Ltd., 720 Cai Lun Road, Building 5, Pudong, Shanghai 201203, P. R. China

[‡]Crown Bioscience Inc., Light Muller Building, Changping Sector of Zhongguancun Science Park, No.21 Huoju Street, Changping District, Beijing 102200, P. R. China

[§]Chipscreen Biosciences Ltd., 2-601, BIO-Incubator, Gaoxin C, first Ave., Shenzhen High-Tech Industrial Park, Nanshan District, Shenzhen, Guangdong 518057, P. R. China

S Supporting Information

ABSTRACT: Herein, we describe the pharmacokinetic optimization of a series of class-selective histone deacetylase (HDAC) inhibitors and the subsequent identification of candidate predictive biomarkers of hepatocellular carcinoma (HCC) tumor response for our clinical lead using patient-derived HCC tumor xenograft models. Through a combination of conformational constraint and scaffold hopping, we lowered the in vivo clearance (CL) and significantly improved the bioavailability (F) and exposure (AUC) of our HDAC inhibitors while maintaining selectivity toward the class I HDAC family with particular potency against HDAC1, resulting in clinical lead **5** (HDAC1 IC₅₀ = 60 nM, mouse CL = 39 mL/min/kg, mouse F = 100%, mouse AUC after single oral dose at 10 mg/kg = 6316 h·ng/mL). We then evaluated **5** in a biomarker discovery pilot study using patient-derived tumor xenograft models, wherein two out of the three models responded to treatment. By comparing tumor response status to compound tumor exposure, induction of acetylated histone H3, candidate gene expression changes, and promoter DNA methylation status from all three models at various time points, we identified preliminary candidate response prediction biomarkers that warrant further validation in a larger cohort of patient-derived tumor models and through confirmatory functional studies.

**INTRODUCTION**

Hepatocellular carcinoma (HCC) is among the leading causes of cancer death worldwide with an overall 5-year median survival rate that remains below 12% in the United States.¹ Most HCC patients are first diagnosed when the disease has reached an advanced and/or unresectable stage where either systemic or local chemotherapy are the standard treatment options.² Currently, systemic treatment with the multitargeted kinase inhibitor sorafenib is considered the standard of care for advanced HCC, providing a median overall survival of 10.7 months as compared to 7.9 months with placebo.³ In light of the poor overall survival rates associated with HCC and the limited efficacy of sorafenib, there is a great need to identify new targets and corresponding drug candidates for HCC treatment.

The histone deacetylases (HDACs) are a family of Zn²⁺-dependent hydrolases that remove the acetyl group from the acetylated ϵ -amino side chain of lysine residues in histones and

in a wide variety of other post-translationally acetylated proteins. The HDAC family of enzymes can be divided into two major groups, the Rpd3/Hda1-like NAD-independent lysine deacetylases and the NAD-dependent sirtuins.⁴ The Rpd3/Hda1-like deacetylase group has been further organized into class I enzymes (HDACs 1, 2, 3, and 8) and class II enzymes (HDACs 4, 5, 6, 7, 9, 10) based on sequence similarity to the yeast HDACs Rpd3 and Hda1, respectively.⁵

With respect to HDACs as potential targets for HCC treatment, HDAC1 in particular has been found to be significantly overexpressed in HCC patient tumor samples and its expression in this context is negatively correlated to overall survival.⁶ Moreover, hepatitis B virus (HBV), which has been strongly implicated in HCC pathogenesis, has been demonstrated to induce HDAC1 overexpression through the

Received: August 11, 2012

Published: October 12, 2012

HBV HBx protein in hepatocellular carcinoma cells, leading to an enhancement of pro-tumor hypoxia signaling.⁷ Functionally, small molecule HDAC inhibition in HCC cells induces antiproliferative and pro-apoptotic effects that correlate with in-cell target inhibition as assessed by classical pharmacodynamic markers such as p21 and acetylated histone H3.^{8,9} Moreover, in certain cellular contexts, HDAC inhibition can reactivate the expression of tumor suppressor genes such as TMS1/ASC¹⁰ and TFPI-2¹¹ that have been epigenetically silenced through promoter CpG island DNA hypermethylation which ultimately recruits multiprotein complexes including HDAC1 to enforce a transcriptionally repressed heterochromatin state.¹² Furthermore, in preclinical in vivo models, HDAC inhibitors can significantly inhibit the growth of established HCC tumors.¹³ As a result of the evidence linking HDAC activity with HCC pathogenesis and progression, several pan-HDAC inhibitors (Figure 1A) are currently in or recently have been in early stage clinical trials in HCC either as single agents or in combination with sorafenib or traditional chemotherapy.¹⁴

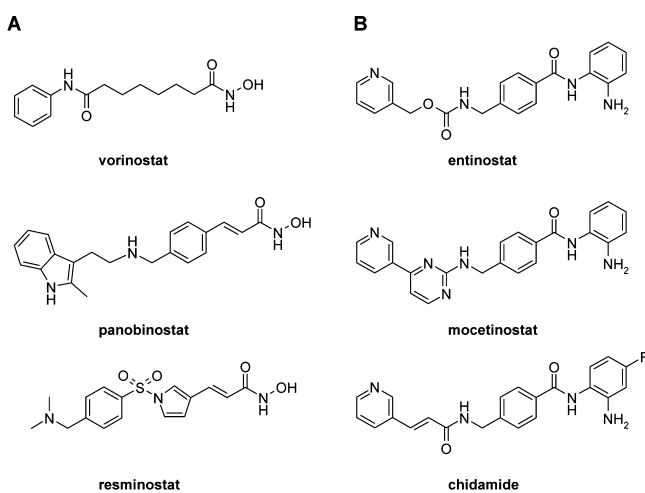


Figure 1. Representative HDAC inhibitors. (A) HDAC inhibitors that have been or are being evaluated in the clinic for HCC therapy; (B) *o*-aminoanilide HDAC inhibitors under clinical development.

On the basis of the evidence implicating HDAC1 in HCC in particular, and in contrast to the pan-HDAC inhibitors currently under clinical evaluation in HCC, we set out to develop a selective class I HDAC inhibitor based on the *o*-aminoanilide pharmacophore¹⁵ (Figure 1B) with particular potency toward HDAC1 for HCC therapy. Furthermore, consistent with our general strategy of developing companion predictive and/or pharmacodynamic biomarkers for our drug discovery programs, we incorporated biomarker hypothesis generation¹⁶ as part of our preclinical candidate research and selection efforts, as detailed below, to ultimately inform and improve our future clinical trial design. In particular, in light of the relatively limited clinical efficacy of HDACi in solid tumor treatment thus far, we envisioned that the identification of predictive biomarkers of tumor response could help guide the selection of HCC patients more likely to benefit from treatment with our class I-selective HDACi in either a monotherapy or combination therapy setting.¹⁷ While other researchers have previously sought to identify predictive biomarkers for HDACi in various cell models and/or clinical isolates,¹⁸ to our knowledge the research disclosed herein is the

first published example employing mRNA and DNA methylation profiling in patient-derived xenograft models to identify candidate predictive biomarkers of HCC tumor response for a class I-selective HDAC inhibitor.

We previously identified compound **1** (Figure 2) as an *o*-aminoanilide-based selective class I HDAC inhibitor with particular potency against HDAC1 and good cell-based activity as assessed by p21 reporter gene assay, endogenous p21 and acetylated histone H3 induction assays, and antiproliferative assays in various cancer cell lines.¹⁹ While **1** and its closely related analogues had reasonable enzyme- and cell-based activities, these compounds were not suitable for further drug candidate development due to high in vivo clearance and limited bioavailability. We therefore undertook a two-stage campaign to optimize compound **1**. In the first stage, we attempted to replace the conformationally flexible and metabolically labile morpholine side chain with more compact and rigid moieties to balance the overall properties of our lead series. In the second stage, motivated by the modest, but still suboptimal, property improvement attained by replacing the morpholine side chain, we further rigidified our lead structure through a scaffold-hopping approach.²⁰ This two-staged effort ultimately led to the discovery of clinical candidate compound **5** and its evaluation in primary patient tumor-derived HCC xenograft models for the identification of candidate predictive tumor response biomarkers, as detailed below.

CHEMISTRY

General Comments on Stereochemistry. Unless otherwise noted, compounds were synthesized as racemic mixtures.

General Synthesis of Morpholine Side-Chain Replacement Analogues of Compound **1 (Scheme 1).** Synthesis of morpholine side-chain replacement analogues of compound **1** began with esterification of commercially available 2-(4-bromophenyl)-2-hydroxyacetate in methanol with sulfuric acid as catalyst to obtain methyl ester **I**. Subsequent Heck coupling of **I** with acrylamide **III** (obtained by acylation of Boc-protected aniline **II** with the mixed anhydride of acrylic acid) using tri-*o*-tolylphosphine as ligand provided cinnamide **IV** in moderate yield. Mesylation of **IV** followed by nucleophilic substitution on the resulting mesylates with alkyl amines gave α -amino esters which were hydrolyzed to the corresponding acids and then coupled with various amines using carbodiimide chemistry to obtain α -amino amides **VI**. Final Boc group deprotection in methanolic HCl gave target compounds **2–4** and **6–10** (see Supporting Information Table S1).

General Synthesis of R¹ Analogues of the *rac*-(*trans*-3,4)-Disubstituted Pyrrolidine Series (Scheme 2). Synthesis of R¹ analogues of the *rac*-(*trans*-3,4)-disubstituted pyrrolidine series began with iminium ylide cycloaddition²¹ of commercially available (*E*)-3-(4-bromophenyl)acrylic acid ethyl ester with sarcosine and paraformaldehyde to obtain pyrrolidine **VII**. Pyrrolidine **VII** was then reacted with acrylamide **III** using Heck coupling conditions as described above to synthesize cinnamide **VIII**. Hydrolysis of **VIII** using lithium hydroxide in methanol furnished the corresponding carboxylic acid which was then coupled with various amine/aniline building blocks and subsequently subjected to methanolic HCl to provide final compounds **11–42** as racemic mixtures of *trans* diastereomers.

General Synthesis of R² Analogues of the *rac*-(*trans*-3,4)-Disubstituted Pyrrolidine Series via Alkylation, Epoxidation, Reductive Amination, Acylation, or Nucleophilic Substitution (Scheme 3). Synthesis of R² analogues

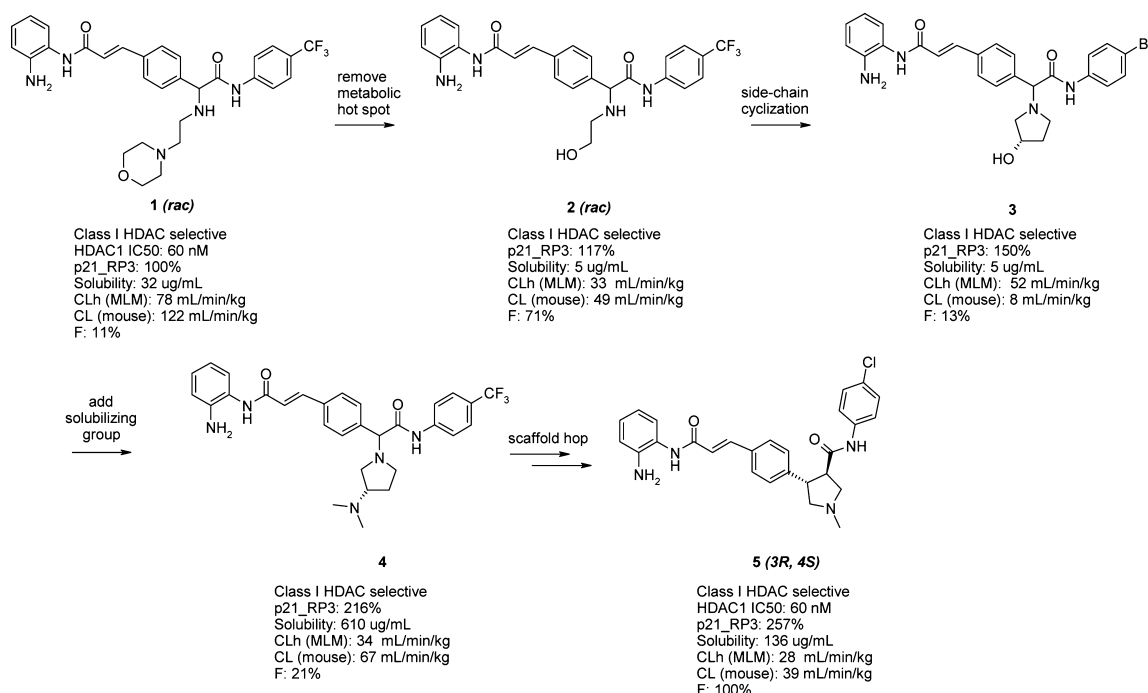
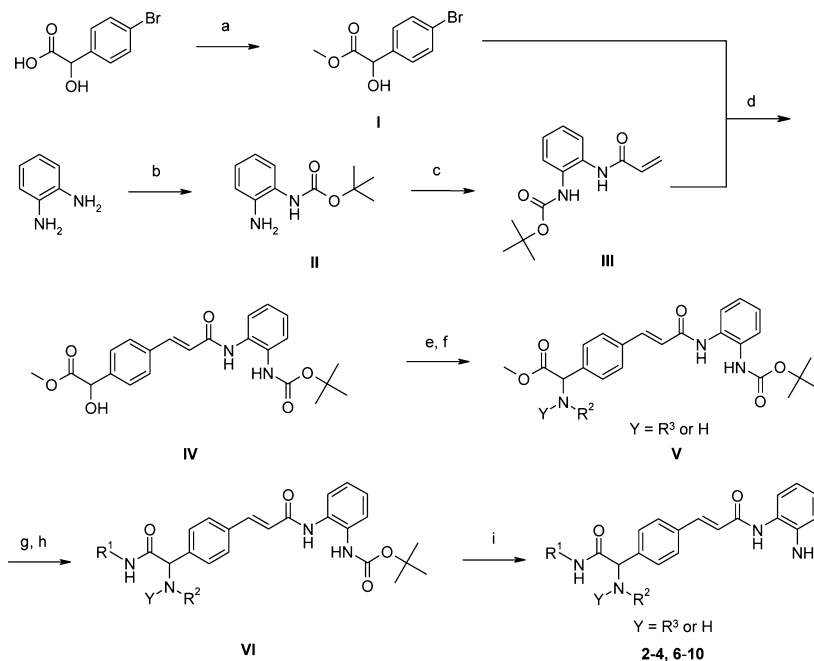


Figure 2. Summary of compound **1** optimization history leading to identification of clinical lead **5** and the associated *trans*-3,4-disubstituted pyrrolidine lead series. P21_RP3 is the relative fold increase in luciferase signal in the p21 reporter gene assay compared to clinical HDACi entinostat (both test compound and comparator were evaluated at 3 μ M in duplicate or triplicate) and normalized by internal GFP transfection control. CLh (MLM) is the calculated hepatic clearance based on mouse liver microsome intrinsic clearance. CL (mouse) is the in vivo systemic clearance measured by intravenous pharmacokinetic study in BALB/C nude mice. F is the bioavailability determined by single dose intravenous (2 mpk) and oral (10 mpk) pharmacokinetic study in nude mice. See Experimental Section for further details.

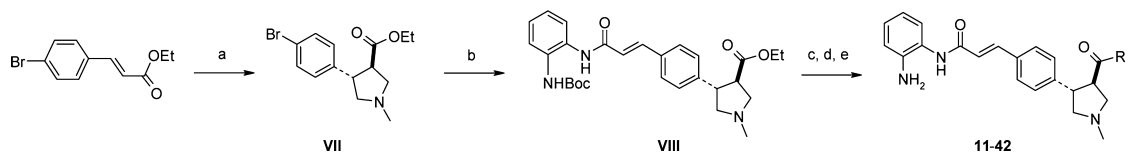
Scheme 1. Synthesis Morpholine Side-Chain Replacement Analogues of Compound 1^a



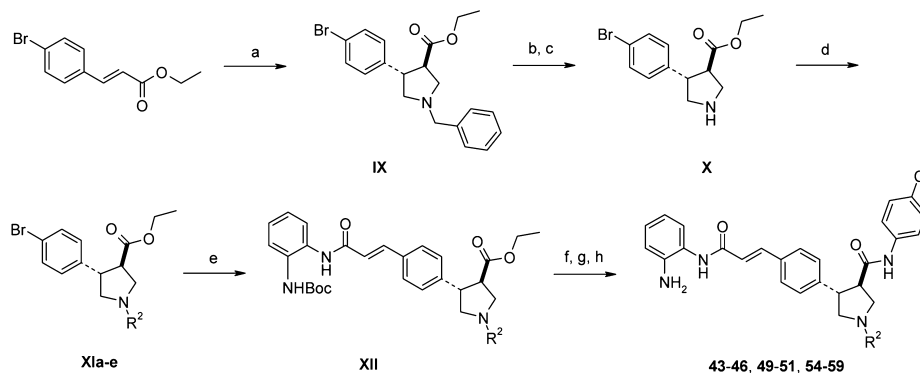
^a(a) H₂SO₄, MeOH, 50 °C, 3 h, 77%; (b) Boc₂O, THF, rt, 16 h, 77%; (c) acrylic acid, *N*-methylmorpholine, isobutyl chloroformate, DCM, 0 °C, 30 min and then add intermediate **II** at reflux over 30 min, stir 2 h, 34%; (d) tri-*o*-tolylphosphine, TEA, Pd₂(dba)₃, DMF, 100 °C, 6 h, 60%; (e) MsCl, TEA, DCM, 0 °C, 1 h; (f) R²NH₂ or R²R³NH, TEA, DCM, rt, 16 h; (g) LiOH, MeOH, rt, 5 h, 81% (three steps); (h) R¹NH₂, PyBrop, DIPEA, DCM, rt, 12 h; (i) 1.25 M HCl in MeOH, rt, 2 h, and then NaHCO₃, 20–25% (two steps).

of the *rac*-(*trans*-3,4)-disubstituted pyrrolidine series in which the R² group was installed via alkylation, epoxidation, reductive amination, acylation, or nucleophilic substitution began with

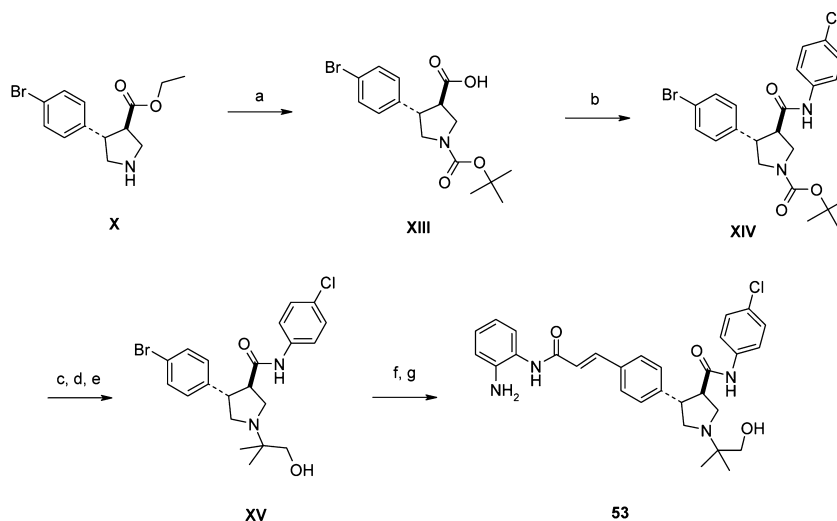
orthoboric acid-catalyzed iminium ylide cycloaddition of commercially available (*E*)-3-(4-bromophenyl)acrylic acid ethyl ester with *N*-(methoxymethyl)-*N*-(trimethylsilylmethyl)-

Scheme 2. Synthesis of R¹ Analogues of the *rac*-(*trans*-3,4)-Disubstituted Pyrrolidine Series^a

^a(a) Sarcosine, paraformaldehyde, toluene, reflux, 4 h, 46%; (b) **III**, Pd₂(dba)₃, tri-*o*-tolylphosphine, TEA, DMF, 110 °C (sealed tube), 16 h, 87%; (c), LiOH, MeOH, rt, 16 h; (d) R¹ (substituted amine, aniline, or aminopyridine), HATU, TEA, DMF:DCM (1:10), rt, 3 h, 88% (two steps); (e) 1 N HCl in MeOH, rt, 4 h, 43%.

Scheme 3. Synthesis of R² Analogues of the *rac*-(*trans*-3,4)-Disubstituted Pyrrolidine Series via Alkylation, Epoxidation, Reductive Amination, Acylation, or Nucleophilic Aromatic Substitution^a

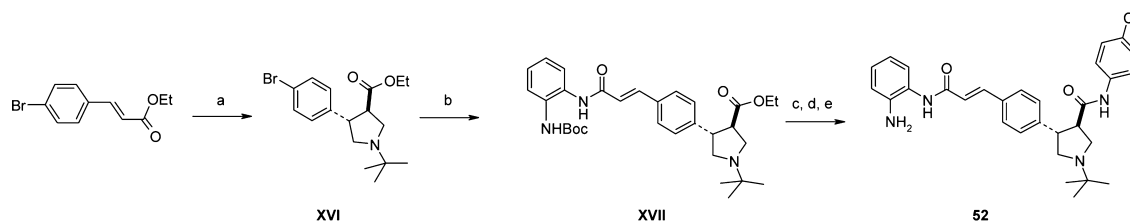
^a(a) *N*-(Methoxymethyl)-*N*-(trimethylsilylmethyl)benzylamine, orthoboric acid, DCM, rt, 2 d then 45 °C for 2 h, 71%; (b) 2,2,2-trichloroethyl chloroformate, K₂CO₃, CH₃CN, 60 °C, 3 h, 66%; (c) Zn, acetic acid, rt, 3 h; (d) for alkylation (R²X where X is halide, tosylate, or mesylate): K₂CO₃, KI, R²X, DMF, 130 °C (microwave) 20 min; for epoxidation (2,2-dimethyloxirane): 2,2-dimethyloxirane, EtOH, 80 °C (sealed tube), 5 h, 96%; for reductive amination (R² = R³R⁴CH after reduction from R³R⁴CO): R³R⁴CO, NaBH(OAc)₃, catalytic acetic acid, MeOH, rt, 16 h, 64%; for acylation: triphosgene and R³R⁴NH (R² = CONR³R⁴), DIPEA, THF, 0 °C to rt, 12 h; for nucleophilic aromatic substitution (2-chloropyrimidine): 2-chloropyrimidine, DIPEA, *i*-PrOH, 130 °C (microwave), 10 min, 60%; (e) *N*-(2-(acryloylamino)phenyl)carbamic acid *tert*-butyl ester (**III**), Pd₂(dba)₃, tri-*o*-tolylphosphine, TEA, DMF, 100 °C, 3 h; (f) R¹ (substituted amine, aniline, or aminopyridine), LiOH, MeOH, rt, 16 h; (g) HATU, TEA, DMF:DCM (1:10), rt, 3 h; (h) 1 N HCl in MeOH, rt, 4 h.

Scheme 4. Synthesis of the *rac*-(*trans*-3,4)-Disubstituted Pyrrolidine Series Analogue 53 (R² = 2-hydroxy-1,1-dimethylethyl)^a

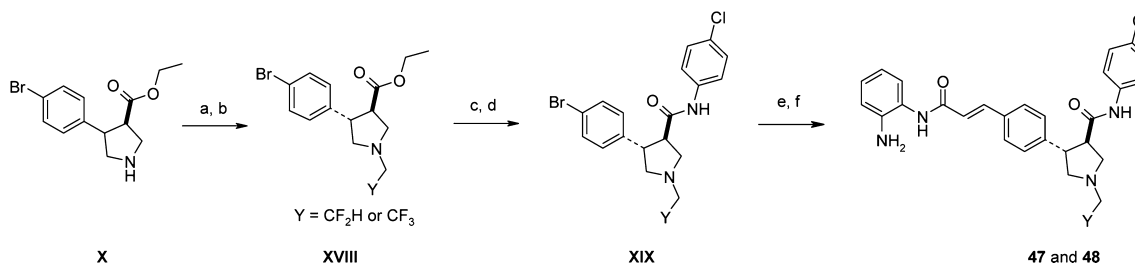
^a(a) NaOH, CH₃CN, rt, 2 h then Na₂CO₃, Boc₂O, rt, 16 h, 50%; (b) 4-chloroaniline, HOBT, EDCI, DCM, rt, 16 h; (c) 1.25 M HCl in MeOH, rt, 3 h then Na₂CO₃; (d) 2-bromo-2-methylpropionic acid methyl ester, K₂CO₃, DMF, 50 °C, 5 h; (e) LiBH₄, THF, rt, 2 h (17%, four steps); (f) *N*-(2-(acryloylamino)phenyl)carbamic acid *tert*-butyl ester (**III**), Pd₂(dba)₃, tri-*o*-tolylphosphine, TEA, DMF, 100 °C, 3 h; (g) 1.25 M HCl, MeOH, rt, 3 h (24%, two steps).

benzylamine in DCM to afford *N*-benzylpyrrolidine **IX**. Except for the synthesis of final compound **58**, where *N*-benzyl pyrrolidine **IX** was directly reacted with acrylamide **III** to obtain cinnamide **XII**, the *N*-benzyl group was then removed in

a two-step process involving conversion of the *N*-benzyl group to trichloroethyl carbamate with trichloroethyl chloroformate followed by carbamate cleavage mediated by zinc metal in acetic acid to provide pyrrolidine **X**. Pyrrolidine **X** was then

Scheme 5. Synthesis of *rac*-(*trans*-3,4)-Disubstituted Pyrrolidine Analogue 52 ($R^2 = \textit{tert}$ -butyl)^a

^a(a) *N*-*tert*-butylglycine hydrochloride, paraformaldehyde, toluene, reflux, 4 h, 12%; (b) *N*-(2-(acryloylamino)phenyl)carbamic acid *tert*-butyl ester (**III**), Pd₂(dba)₃, tri-*o*-tolylphosphine, TEA, DMF, 110 °C (sealed tube), 12 h, 53%; (c) LiOH, THF, rt, 16 h; (d) 4-chloroaniline, HATU, TEA, DCM, rt, 16 h, 66% (two steps); (e) 1.25 M HCl in MeOH, rt, 4 h, 27%.

Scheme 6. Synthesis of *rac*-(*trans*-3,4)-Disubstituted Pyrrolidine Analogues 47 and 48 ($R^2 = 1,1$ -difluoroethyl and 1,1,1-trifluoroethyl)^a

^a(a) For Y = CF₃: triflic anhydride, TEA, DCM, 0 °C, 30 min and then to rt, 1 h, 68%; for Y = CF₂H: difluoroacetyl chloride, DCM, rt, 1 h, 97%; (b) for Y = CF₃: BH₃, THF, 0 °C, 2 h, 30%; for Y = CF₂H: BH₃, THF, 60 °C, 5 h, 63% (c) NaOH H₂O/MeOH, rt, 4 h; (d) 4-chloroaniline, PyBrop, DIPEA, DCM, rt, 16 h, 90%; (e) *N*-(2-(acryloylamino)phenyl)carbamic acid *tert*-butyl ester (**III**), Pd₂(dba)₃, tri-*o*-tolylphosphine, TEA, DMF, 110 °C (sealed tube), 4 h, 86%; (f) TFA, DCM, rt, 2 h.

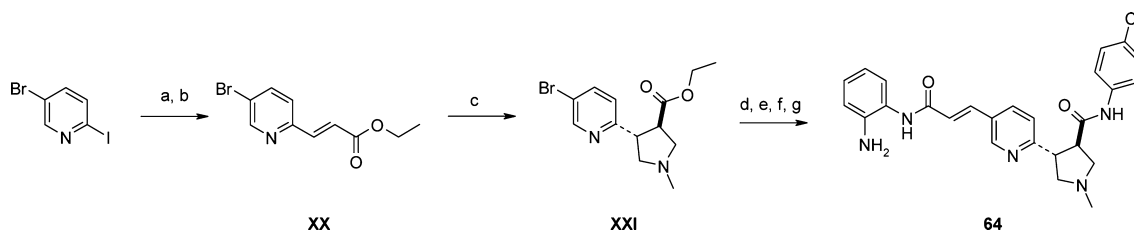
converted to R^2 -substituted pyrrolidine **XI** via one of five general methods depending on the nature of the R^2 substituent. To obtain the R^2 -substituted pyrrolidines **XIa** corresponding to final compounds **45**, **46**, **49**, **50**, and **54**, pyrrolidine **X** was alkylated under microwave conditions with potassium iodide as catalyst with various R^2X building blocks, where **X** was a suitable leaving group such as bromide or tosylate. Over-alkylation was generally not an issue in these cases presumably due to the deactivating effect that these R^2 substituents had on the nucleophilicity of the resulting tertiary pyrrolidine amine. To obtain the corresponding pyrrolidine intermediate (**XIb**) for compound **51**, pyrrolidine **X** underwent S_N2 reaction with 2,2-dimethyloxirane in ethanol. For pyrrolidine intermediates **XIc** corresponding to final compounds **43**, **44**, and **59**, pyrrolidine **X** underwent reductive amination with acetaldehyde, acetone, and tetrahydropyran-4-one, respectively. For the pyrrolidine intermediate **XId** corresponding to final compounds **55** and **56**, pyrrolidine **X** was acylated with triphosgene and the appropriate alkyl amine. For the pyrrolidine intermediate **XIe** corresponding to final compound **57**, pyrrolidine **X** underwent nucleophilic aromatic substitution with 2-chloropyrimidine. Pyrrolidine intermediates **XIa–e** from all five general methods were then coupled with acrylamide **III** via the Heck conditions described above to obtain cinnamide esters **XII**. Esters **XII** were then hydrolyzed to the corresponding cinnamide acids with lithium hydroxide in methanol followed by HATU-mediated condensation with 4-chloroaniline and final deprotection in methanolic HCl to afford final compounds **43–46**, **49–51**, and **54–59** as racemic mixtures of *trans* diastereomers.

Synthesis of *rac*-(*trans*-3,4)-Disubstituted Pyrrolidine Analogue 53 ($R^2 = 2$ -hydroxy-1,1-dimethylethyl) (Scheme 4). Synthesis of compound **53** began with one-pot hydrolysis and Boc protection of pyrrolidine ester **X** to obtain

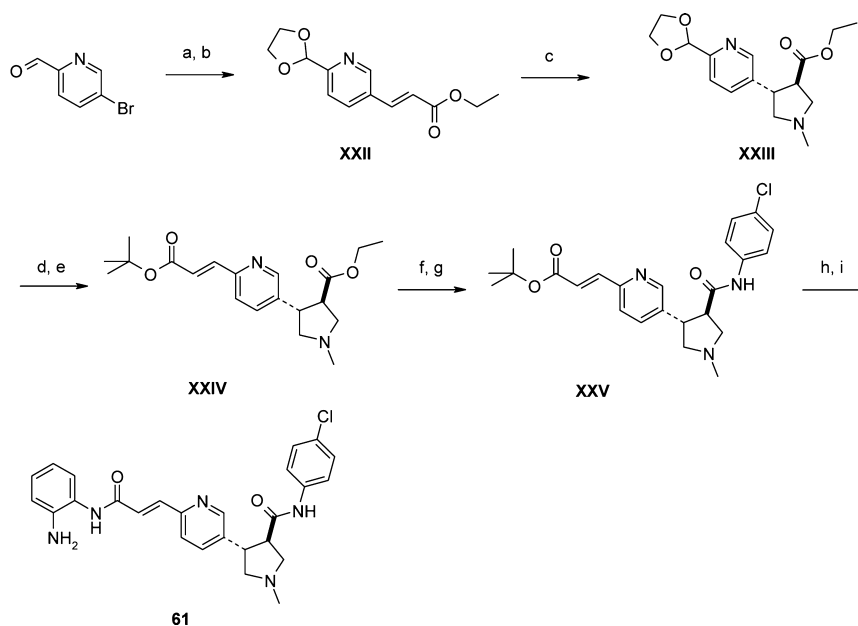
the pyrrolidine acid **XIII**. Carbodiimide-mediated coupling of 4-chloroaniline with acid **XIII** furnished pyrrolidine amide **XIV**. Amide **XIV** was deprotected in methanolic HCl to yield pyrrolidine amine HCl salt, which was then reacted with 2-bromo-2-methylpropionic acid methyl ester in DMF and subsequently reduced with lithium borohydride in THF to the corresponding alcohol **XV**. Heck coupling of acrylamide **III** with **XV** provided the corresponding cinnamide which was then deprotected in methanolic HCl to give compound **53**.

Synthesis of *rac*-(*trans*-3,4)-Disubstituted Pyrrolidine Analogue 52 ($R^2 = \textit{tert}$ -butyl) (Scheme 5). Synthesis of compound **52** began with iminium ylide cycloaddition of commercially available (*E*)-3-(4-bromophenyl)acrylic acid ethyl ester with *N*-*tert*-butylglycine hydrochloride salt and paraformaldehyde in refluxing toluene to obtain *N*-*tert*-butylpyrrolidine **XVI**. Heck coupling of **XVI** with acrylamide **III** then furnished cinnamide ester **XVII**. Ester **XVII** was hydrolyzed with lithium hydroxide in THF, then the corresponding acid underwent HATU-mediated coupling with 4-chloroaniline followed by Boc deprotection with methanolic HCl to obtain final compound **52**.

Synthesis of *rac*-(*trans*-3,4)-Disubstituted Pyrrolidine Analogues 47 and 48 ($R^2 = 1,1$ -difluoroethyl and 1,1,1-trifluoroethyl) (Scheme 6). Synthesis of compounds **47** and **48** began with acylation of pyrrolidine **X** with difluoroacetyl chloride and triflic anhydride, respectively, followed by selective amide reduction with borane in THF to yield the corresponding *N*-alkyl pyrrolidines **XVIII**. *N*-Alkyl pyrrolidines **XVIII** were then treated with lithium hydroxide followed by PyBrop-mediated coupling of 4-chloroaniline to the resulting acids to obtain pyrrolidine amides **XIX**. These pyrrolidine intermediates **XIX** then underwent Heck coupling with

Scheme 7. Synthesis of *rac*-(*trans*-3,4)-Disubstituted Pyrrolidine 5-Vinylpyridin-2-yl Linker Analogue 64^a

^a(a) *i*-PrMgCl, THF, -20°C , 2 h and then add DMF, 0°C to rt, 1 h, 90%; (b) triethyl phosphonoacetate, TEA, LiBr, CH_3CN , rt, 16 h, 67%; (c) sarcosine, paraformaldehyde, toluene, reflux, 4 h, 77%; (d) *N*-(2-(acryloylamino)phenyl)carbamic acid *tert*-butyl ester (III), $\text{Pd}_2(\text{dba})_3$, tri-*o*-tolylphosphine, TEA, DMF, 100°C , 3 h, 75%; (e) LiOH, THF/ H_2O (3:1), rt, 5 h, 86%; (f) 4-chloroaniline, HATU, TEA, DCM, rt, 16 h, 54%; (g) 2 N HCl, MeOH, rt, 4 h.

Scheme 8. Synthesis of *rac*-(*trans*-3,4)-Disubstituted Pyrrolidine 6-Vinylpyridin-3-yl Linker Analogue 61^a

^a(a) Ethane-1,2-diol, TsOH, toluene, reflux, 6 h; (b) ethyl acrylate, $\text{Pd}_2(\text{dba})_3$, tris-*o*-tolylphosphine, TEA, 110°C , 3 h; (c) *N*-methylglycine, paraformaldehyde, toluene, reflux, 6 h; (d) LiCl, DMSO/ H_2O (3:1), 150°C (microwave), 10 min; (e) diethyl *tert*-butyl phosphonoacetate, *n*-butyllithium, THF, -78 to 0°C , 2 h; (f) LiOH, THF/ H_2O (3:1), rt, 3 h; (g) 4-chloroaniline, HATU, TEA, DCM, rt, 24 h; (h) TFA, DCM, 0°C to rt, 2 h; (i) 1,2-diaminobenzene, HATU, TEA, DCM, rt, 12 h.

acrylamide III followed by Boc deprotection in methanolic HCl to afford final compounds 47 and 48.

Synthesis of *rac*-(*trans*-3,4)-Disubstituted Pyrrolidine 5-Vinylpyridin-2-yl Linker Analogue 64 (Scheme 7). Synthesis of compound 64 began with isopropyl magnesium chloride-mediated formylation of 5-bromo-2-iodopyridine with DMF followed by HWE reaction to furnish substituted ethyl acrylate XX. Iminium ylide cycloaddition of ethyl acrylate XX with sarcosine and paraformaldehyde in refluxing toluene produced the *N*-methyl pyrrolidine ester XXI. Intermediate XXI was then converted to final compound 64 in a series of transformations analogous to those for the conversion of intermediate XI to *rac*-(*trans*-3,4)-disubstituted pyrrolidine R^2 analogues (Scheme 3).

Synthesis of *rac*-(*trans*-3,4)-Disubstituted Pyrrolidine 6-Vinylpyridin-3-yl Linker Analogue 61 (Scheme 8). Synthesis of compound 61 began with protection of 4-bromobenzaldehyde as its [1,3]dioxolane acetal followed by Heck reaction with ethyl acrylate to furnish substituted ethyl acrylate XXII. Iminium ylide cycloaddition of XXII with

sarcosine and paraformaldehyde in refluxing toluene yielded *N*-methylpyrrolidine XXIII. Removal of the acetal protecting group using lithium chloride in a DMSO– H_2O solvent system under microwave conditions furnished the corresponding aldehyde which was then converted to (*E*)-3-pyridin-2-ylacrylic acid *tert*-butyl ester XXIV via HWE reaction with diethyl *tert*-butyl phosphonoacetate. Selective lithium hydroxide-mediated hydrolysis of the ethyl ester followed by HATU-mediated coupling to 4-chloroaniline gave pyrrolidine amide XXV. Cleavage of the *tert*-butyl ester with TFA followed by coupling to 1,2-diaminobenzene using HATU furnished target compound 61.

Synthesis of Compounds 5, 60, 62, and 63. Schemes and experimental methods for the synthesis of *rac*-(*trans*-3,4)-disubstituted pyrrolidine 2-fluoro-4-vinylphenyl linker analogue 60, *rac*-(*trans*-3,4)-disubstituted pyrrolidine 5-vinylpyrazin-2-yl linker analogue 62, and *rac*-(*trans*-3,4)-disubstituted pyrrolidine 5-vinylpyridazin-2-yl linker analogue 63 can be found in the Supporting Information. A scheme and experimental methods for the enantioselective synthesis of compounds 5 (3*R*,4*S*) and

65 (3*S*,4*R*), the corresponding enantiomers of *rac*-(*trans*-3,4)-disubstituted pyrrolidine **15**, are available in the Supporting Information.

RESULTS AND DISCUSSION

Lead Optimization Process and Parameters. We selected the p21 reporter gene assay and liver microsomal stability assay as a primary screening system to guide our medicinal chemistry efforts because the goal of our optimization campaign was to improve compound metabolic stability while maintaining in-cell activity against the class I HDACs comparable or superior to entinostat (Figure 1B), a clinical stage *o*-aminoanilide HDAC inhibitor. Representative compounds from structurally distinct subseries were also tested in a solubility assay to focus optimization efforts on subseries with comparable or improved solubility relative to **1** so as to broaden future formulation and dosing administration options. Compounds with good in-cell HDAC inhibitory activity, comparable or improved solubility relative to **1**, and improved in vitro metabolic stability were then assessed in single-dose intravenous and oral pharmacokinetic studies in rodents (mostly BALB/C nude mice). Compounds with good pharmacokinetic profiles were then further prioritized through cytochrome P450 (CYP) and human ether-à-go-go-related gene (hERG) counter-screening. The optimized leads arising from this process were then spot-checked in a cell-free biochemical HDAC inhibition panel before proceeding to in vivo efficacy and biomarker studies.

Modification of the Morpholine Side Chain. Metabolite identification studies indicated that the 2-morpholin-4-ylethylamino side chain is a major site of oxidative metabolism for compound **1** (see Supporting Information for details). We initially explored two approaches to reduce oxidative metabolism at this site: (1) replacement of the morpholine moiety; (2) conformational restriction of the alkyl amino side chain. Whereas replacement of the morpholine moiety with a simple primary hydroxyl group to generate **2** led to improved microsomal stability (Figure 2), not surprisingly the removal of the basic amine also lowered compound solubility. Alternatively, side-chain cyclization (compound **3**) combined with addition of a solubilizing dialkylamino group to give **4** led to both improved in vitro metabolic stability and vastly improved solubility (Figure 2). Notably, five-membered ring cyclization was found to be superior to four- or six-membered ring cyclization in terms of p21 induction activity (see compounds **6–10** in Supporting Information Table S1). Despite the improved in vitro metabolic stability and solubility of **4**, this compound still had high in vivo clearance, albeit lower than compound **1** (Figure 2). Therefore, our subsequent efforts focused on a distinct *trans*-3,4-disubstituted pyrrolidine-based scaffold inspired by our previous experience with the *trans*-3,4-disubstituted pyrrolidine core in another lead optimization program and supported by docked conformational alignment modeling with **4** (Figure 3).

Systematic *trans*-3,4-Disubstituted Pyrrolidine Optimization. As briefly summarized above, due to the difficulties we encountered in optimizing either compound **1** or its side-chain-cyclized analogues, we focused the majority of our efforts on systematically exploring and optimizing the *trans*-3,4-disubstituted pyrrolidine scaffold. In this respect, we sequentially varied the R¹, R², and linker (L) positions (Figure 4) to identify an optimal combination of R¹, R², and linker substructures to achieve both good in-cell target inhibition

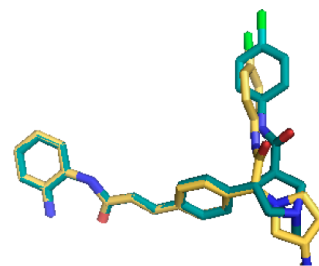


Figure 3. Docked conformational alignment by Glide software (see Experimental Section) of a prototypical *trans*-3,4-disubstituted pyrrolidine scaffold core (blue sticks) with that of the pyrrolidine-based side-chain analogues of **4** (yellow sticks). For clarity, HDAC1 homology model used for docking is not shown.

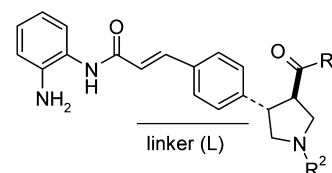


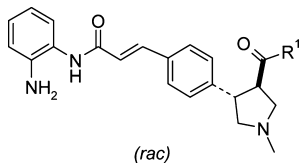
Figure 4. Generalized structure of the *trans*-3,4-disubstituted pyrrolidine series.

and a pharmacokinetic profile suitable for in vivo efficacy and biomarker studies.

R¹ Position SAR. Our optimization effort began with the exploration of various R¹ substituents while fixing R² and the linker region as a simple methyl group and the standard cinnamide linker, respectively. Compounds with aromatic R¹ substituents containing electron-withdrawing groups in the para position of the aromatic ring generally had reasonable in vitro microsomal stability (compounds **12**, **13**, **16**, **19**, **20** in Table 1) whereas the *p*-fluoro and *p*-chloro substituted compounds **12** and **13** were preferred for obtaining both moderate microsomal stability and in-cell target activity. In contrast, meta and ortho monosubstituted aromatic R¹ substituents were well-tolerated in terms of target activity but did not result in good microsomal stability (compounds **21–25**). Combining meta or ortho substituents with *p*-fluoro or *p*-chloro substituents (compounds **26–33**) did not lead to any obvious improvement in activity or microsomal stability as compared to the monosubstituted *p*-fluoro or *p*-chloro derivatives **12** and **13**. Simple pyridinyl R¹ analogues **35** and **37** also displayed reasonable activity and stability, whereas pyridinyl R¹ analogue **34** had decreased in-cell target activity. Finally, we explored various aliphatic R¹ substituents but found that none of these compounds (**39–42**) had both robust in-cell target activity and good microsomal stability. In summary, these results indicated that the optimal choice of substituent for the R¹ position is either a *p*-fluoro- or *p*-chloro-substituted phenyl ring. Accordingly, in our subsequent studies of the R² and linker region SAR, we generally fixed the R¹ position as one of these two substituents.

R² Position SAR. While fixing R¹ and the linker region as a *p*-chloro-substituted phenyl ring and cinnamide linker, respectively, we explored a range of saturated and unsaturated R² substituents (Table 2), with the goal of probing both the steric requirements of this region as well as the effect of modulating the basicity of the pyrrolidine nitrogen on the overall properties of the resulting analogues. In terms of steric requirements, we found that a relatively wide range of substituents were well-tolerated in this region, from simple

Table 1. Structure–Activity and Structure–Property Relationships for *trans*-3,4-Disubstituted Pyrrolidines in the R¹ Region

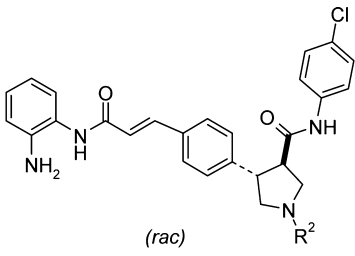


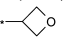
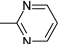
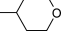
Compound	R ¹		P21 RP3 ^a	HLM ^b	MLM ^b
	X	Y			
11	H	-	270%	7	67
12	F	-	250%	5	34
13	Cl	-	240%	5	35
14	CH ₃	-	260%	15	62
15	OCH ₃	-	170%	14	54
16	CN	-	80%	1	35
17	<i>i</i> -Pr	-	70%	10	54
18	<i>c</i> Pr	-	60%	12	60
19	CF ₃	-	10%	6	23
20	Br	-	40%	3	16
21	F	-	190%	6	56
22	Cl	-	230%	7	58
23	CH ₃	-	350%	14	74
24	OCH ₃	-	170%	14	65
25	F	-	170%	10	67
26	F	F	180%	0	46
27	F	Cl	180%	15	34
28	F	CH ₃	200%	15	62
29	F	Br	200%	15	43
30	Cl	Cl	160%	14	36
31	Cl	CH ₃	210%	15	65
32	F	F	180%	12	27
33	Cl	F	200%	11	43
34	-	-	50%	ND	ND
35	H	-	80%	10	41
36	CH ₃	-	130%	8	57
37	H	-	140%	8	40
38	Cl	-	150%	13	31
39	-	-	70%	8	12
40	-	-	80%	10	7
41	-	-	180%	9	61
42	-	-	10%	9	42

^aP21 RP3 is the relative fold increase in luciferase signal in the p21 reporter gene assay compared to clinical HDACi entinostat (both test compound and comparator were evaluated at 3 μ M in duplicate or triplicate) and normalized by internal GFP transfection control. ^bHLM and MLM are the human and mouse hepatic clearance in units of mL/min/kg as calculated from the intrinsic microsome clearance (see Experimental Section for details).

methyl substitution (compound 13), to *tert*-butyl (compound 52), pyrimidinyl (compound 57), and tetrahydropyranyl (compound 59) substitutions. Moreover, electron-withdrawing alkoxy substituents (for example, compounds 49, 51, 53) were also generally well-tolerated in terms of both in-cell target activity and microsomal stability. In contrast, acyl substituents such as those found in compounds 55 and 56 were less well-tolerated, either leading to suboptimal p21 induction activity or poorer microsomal stability, respectively. Overall, we were unable to fully distinguish beneficial from harmful R²

Table 2. Structure–Activity and Structure–Property Relationships for *trans*-3,4-Disubstituted Pyrrolidines in the R² Region



Compound	R ²	P21 RP3 ^a	HLM ^b	MLM ^b
13	-CH ₃	240%	5	35
43	-CH ₂ CH ₃	170%	12	35
44	-CH(CH ₃) ₂	230%	0	38
45		90%	13	42
46	-CH ₂ CH ₂ F	180%	17	51
47	-CH ₂ CHF ₂	90%	16	49
48	-CH ₂ CF ₃	100%	15	35
49	-CH ₂ CH ₂ OH	100%	11	24
50	-CH ₂ CH ₂ OCH ₃	250%	6	72
51	-CH ₂ C(CH ₃) ₂ OH	230%	14	34
52	-C(CH ₃) ₃	160%	8	20
53	-C(CH ₃) ₂ CH ₂ OH	260%	12	40
54	-CH ₂ CN	190%	17	51
55	-CONHCH ₂ CH ₃	40%	9	25
56	-CON(CH ₂ CH ₃) ₂	90%	19	83
57		120%	11	44
58	-CH ₂ Ph	70%	3	81
59		220%	12	44

^aP21 RP3 is the relative fold increase in luciferase signal in the p21 reporter gene assay compared to clinical HDACi entinostat (both test compound and comparator were evaluated at 3 μ M in duplicate or triplicate) and normalized by internal GFP transfection control. ^bHLM and MLM are the human and mouse hepatic clearance in units of mL/min/kg as calculated from the intrinsic microsome clearance (see Experimental Section for details).

modifications on the basis of in vitro assays alone, so we selected representative R² analogues with good p21 induction activity and microsomal stability for single-dose pharmacokinetic evaluation (see below).

Linker Region SAR. While fixing R¹ and R² as a *p*-chloro-substituted phenyl ring and simple methyl group, respectively, we explored various fine-tuning modifications of the cinnamoyl phenyl ring in the linker region (L), including a nitrogen walk (compounds 61–64) and fluorine substitution (compound 60) (Table 3). Because these relatively conservative changes were all well-tolerated in terms of both in-cell target activity and microsomal stability, we selected representative compounds for single-dose pharmacokinetic evaluation (see below).

Pharmacokinetic Evaluation of Representative *trans*-3,4-Disubstituted Pyrrolidines. We selected 14 *trans*-3,4-disubstituted pyrrolidines, with various R¹, R², and linker region moieties for intravenous and oral single-dose pharmacokinetic studies (Table 4) based on the aforementioned in vitro SAR results. Compounds 12, 44, 63, and 64 had particularly high in vivo clearance generally associated with low to moderate exposure. We presumed that the high in vivo clearance of these compounds was due to clearance pathways acting on these compounds that were not present in the in vitro microsomal assay system. Compounds 53 and 59 had moderate in vivo

Table 3. Structure–Activity and Structure–Property Relationships for Linker Variation (L) within the *trans*-3,4-Disubstituted Pyrrolidine Scaffold

Compound	L	P21 RP3 ^a	HLM ^b	MLM ^b
60		130%	14	36
61		>300%	12	38
62		>300%	11	25
63		>300%	12	41
64		~100% ^c	6	36

^aP21 RP3 is the relative fold increase in luciferase signal in the p21 reporter gene assay compared to clinical HDACi entinostat (both test compound and comparator were evaluated at 3 μ M in duplicate or triplicate) and normalized by internal GFP transfection control. ^bHLM and MLM are the human and mouse hepatic clearance in units of mL/min/kg as calculated from the intrinsic microsome clearance (see Experimental Section for details). ^cEstimated to be at least 100% based on 4-F-phenyl analogue and SAR correlation between 4-F-phenyl and 4-Cl-phenyl subseries (data not shown).

Table 4. Pharmacokinetic Parameters for Selected *trans*-3,4-Disubstituted Pyrrolidines with Acceptable p21 Activity and Mouse Liver Microsome Stability

compound ^a	T_{\max} (h)	C_{\max} (ng/mL)	$T_{1/2}$ (h)	AUC (h·ng/mL)	CL (mL/min/kg)	V_{ss} (L)	F (%)
12	2	170	5.0	624	127	16	95
13	1	324	14	2946	39	8.6	75
5 (3 <i>R</i> ,4 <i>S</i>)	0.25	893	3.4	6316	39	6.9	100
65 (3 <i>S</i> ,4 <i>R</i>)	1	450	6.2	2544	58	9.2	89
26	1	262	4.0	911	53	7.2	29
44	2	331	5.4	2077	86	32	100
49	0.25	957	15	7096	20	4.1	58
51	1	1100	6.5	5653	33	3.7	100
52	2	113	6.8	813	60	31	59
53	2	337	1.1	743	27	6.6	12
59	0.17	315	4.9	1002	39	5.6	23
60	2	828	3.4	3566	23	3	49
63	4	33	ND	116	120	19	9
64	0.17	60	4.6	204	79	4	19

^aCompounds were dosed in nude mice at 10 mpk po and 2 mpk iv except for **12** and **64** which were dosed at 5 mpk po and 1 mpk iv and **63** which was dosed in rat rather than nude mouse. More details for PK studies can be found in the Experimental Section.

clearance but relatively low bioavailability resulting in moderate exposure. Compounds **26** and **52** had moderate bioavailability but also moderately high in vivo clearance. In the case of compound **52**, we presumed that the relatively high lipophilicity of this compound ($c\text{LogP} = 5.4$) relative to the other analogues under investigation contributed to its higher-than-expected in vivo clearance. The remaining compounds, **13**, **5** (3*R*,4*S*) and its corresponding enantiomer **65** (3*S*,4*R*), **49**, **51**, and **60**, demonstrated reasonable overall pharmacokinetic properties, resulting in good exposure and prompting us to conduct more detailed in vitro selectivity assays to select

potential preclinical leads for in vivo efficacy and biomarker studies.

In Vitro Selectivity Panel Assessment for Selected *trans*-3,4-Disubstituted Pyrrolidines. To select compounds not only suitable for in vivo efficacy and biomarker studies but also having good potential to ultimately progress to the clinic, we evaluated the CYP and hERG inhibition profiles for the aforementioned compounds **5**, **65**, **49**, **51**, and **60** that had reasonable pharmacokinetic properties (Table 5). Compounds **49** and **51** demonstrated significant inhibition (less than 10 μ M) of several CYP isoforms and were therefore deprioritized. Compounds **5**, **65**, and **60** were found to have acceptable CYP

Table 5. In Vitro Selectivity of Representative *trans*-3,4-Disubstituted Pyrrolidines toward HDACs, CYPs, and hERG

compound	HDAC isoform IC ₅₀ ^a										CYP isoform IC ₅₀ ^b					hERG IC ₅₀ ^c	
	1	2	3	4	5	6	7	8	9	10	11	3A4	2D6	2C9	2C19		1A2
5	0.06	0.25	0.23	13	3.5	>30	>30	>30	16	3.4	14	14	5	29	43	42	10
65	0.14	0.27	0.20	36	1.1	>30	>30	>30	13	1.6	20	21	32	23	43	50	5
60	0.1	0.22	0.23	46	5.3	>30	>30	>30	43	5	>30	4	9	13	21	28	7
49	ND	ND	ND	ND	ND	ND	ND	ND	ND	ND	ND	2	2	3	10	26	15
51	ND	ND	ND	ND	ND	ND	ND	ND	ND	ND	ND	3	0.7	4	7	7	ND

^aHDAC enzyme inhibition assays were performed by Reaction Biology Corporation according to their standard assay protocols (www.reactionbiology.com, see Experimental Section for additional information). ND = not determined. ^bCYP isoform inhibition assays were performed using the LCMS method.³¹ ^chERG inhibition assay was performed using PatchXpress methodology.³² All IC₅₀ measurements are reported in units of μ M. ND = not determined.

inhibition profiles and were thus assessed in an HDAC isoform panel selectivity assay. Consistent with our expectation of compounds with the *o*-aminoanilide zinc-binding group, these molecules were confirmed to be selective inhibitors of HDAC isoforms 1, 2, and 3. Moreover, compound **5** was particularly active toward HDAC1. Therefore, based on the overall in vitro and in vivo properties of **5**, **65**, and **60**, we selected compound **5** as our lead for in vitro and in vivo efficacy and biomarker studies as well as further preclinical development.

In Vitro Efficacy and Mechanistic Studies of Compound 5. While the intended primary indication for our class I HDAC-selective inhibitors was hepatocellular carcinoma, we decided to use both hepatocellular carcinoma (HCC) and gastric cancer (GC) cell lines to increase our confidence in the basic in vitro efficacy and cell-based mechanistic and functional studies for **5**. Therefore, the antiproliferative activity of **5** was evaluated in a panel of HCC and GC cell lines, using the clinical HDAC inhibitor entinostat and the FDA-approved HDAC inhibitor vorinostat as comparators. As assessed by the concentration required to inhibit 90% of cell growth at 72 h, **5** demonstrated better antiproliferative activity than either entinostat or vorinostat in all cell lines tested (Table 6). Mechanistically, the antiproliferative effect of **5** correlated with the dose-dependent induction of endogenous acetylated histone H3 and p21 after 24 h treatment within a concentration range consistent with the GI₉₀ observed in the same cell line (Figure 5A). Functionally, induction of endogenous acetylated histone H3 and p21 corresponded with a dose-dependent

Table 6. Antiproliferative Activity of Compound **5** versus Clinical Comparators Entinostat and Vorinostat in Asian Hepatocellular Carcinoma and Gastric Cancer Cell Lines

cell line	5 (GI ₉₀) ^a	entinostat (GI ₉₀) ^a	vorinostat (GI ₉₀) ^a
SMMC-7721	1.9	11	20
BEL-7402	1.2	8	17
BEL-7404	3.8	>30	18
SKHEP1	2.5	13	17
QGY-7701	1.3	>30	>30
SGC-7901	1.4	2.5	9.4
MGC8-03	2	8.9	10.8
BGC-823	2.2	7.1	7.5
HGC-27	1	>30	>30

^aGI₉₀ is the concentration (reported in μ M) required to inhibit cell growth by 90% after 72 h compound treatment using the water-soluble tetrazolium (WST) dye assay with eight-point dose–response (half-log serial dilutions in triplicate). See Experimental Section for further details.

decrease in S phase cells at 24 h (consistent with G₁/G₂ cell cycle arrest typically observed for HDAC inhibitors) and subsequent induction of apoptosis at 48 h (representative cell lines, Figure 5B and 5C). Taken together, these results demonstrate that the potent antiproliferative efficacy of **5** is due to HDAC-dependent in-cell induction of histone acetylation leading to concomitant increase in the expression of endogenous cyclin-dependent kinase inhibitor p21, ultimately resulting in cell cycle arrest and apoptosis.

In Vivo Efficacy and PK/PD Studies of 5. Having demonstrated that **5** can potently inhibit HCC and GC cancer cell growth in vitro, we next set out to assess its tumor growth inhibitory effects in subcutaneous cell line and primary tumor-derived xenograft models.

We first evaluated **5** in the HCC cell line-derived xenograft model BEL-7404. At an oral dose of 50 mg/kg once daily or 100 mg/kg every other day, **5** significantly inhibited the growth of established BEL-7404 tumors (tumor growth inhibition rate >60%) with acceptable body weight loss (less than 10% relative to the mean starting weight of the mice). Terminal pharmacokinetic analysis indicated that both dosing schedules resulted in total trough concentrations of **5** in the tumor that were 4-fold above the in vitro GI₉₀ for the corresponding BEL-7404 cell line. This corresponded to consistent pharmacodynamic induction of acetylated histone H3 in the tumor from zero to 24 h after administration of the last dose of **5**, as assessed by Western blot (Figure 6). Taken together, these results demonstrate that **5** has significant in vivo antitumor activity and, while not ruling out unforeseen off-target effects, suggest that this efficacy is linked to target engagement in the tumor as assessed by pharmacokinetic and pharmacodynamic measurements.

With preliminary in vivo efficacy results for **5** in hand, we proceeded to conduct a pilot study with **5** to assess the feasibility of using primary tumor-derived xenograft models to identify candidate predictive biomarkers that could indicate which tumors (or patients) are more likely to respond to treatment with **5**, with the future goal of developing a companion diagnostic for patient selection. We chose to conduct this pilot study with primary tumor-derived subcutaneous xenograft models because, compared to traditional cell line-derived subcutaneous xenograft models, primary tumor-derived models better reflect the histology of the original patient tumor and are presumably therefore more likely to resemble the genetic and epigenetic status of the original tumor.²⁴

We selected three patient-derived HCC tumor models with different associated clinical and molecular characteristics to

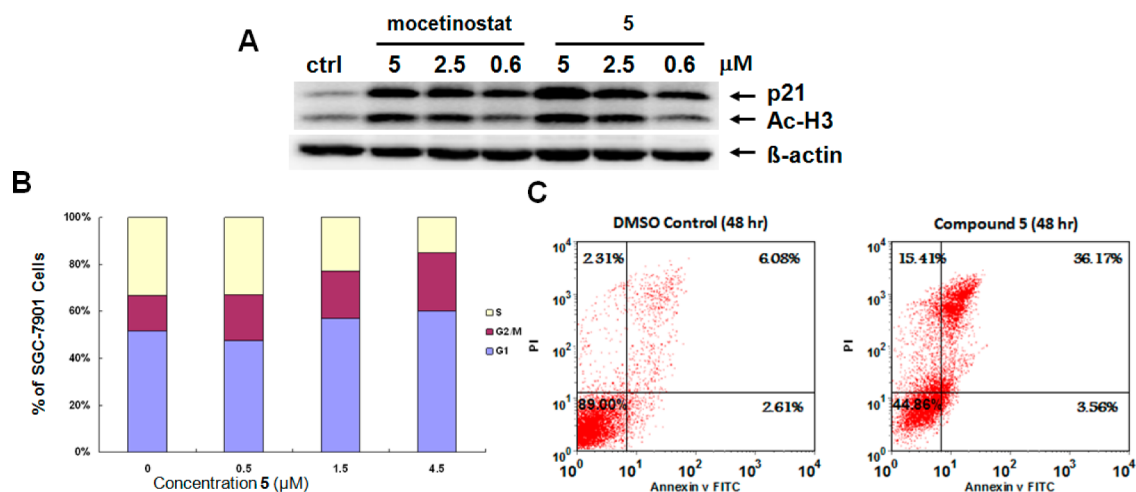


Figure 5. Mechanistic and functional effects of compound 5 in representative hepatocellular carcinoma and gastric cancer cell lines. (A) Dose-dependent induction of endogenous p21 and acetylated histone H3 in response to 24 h treatment with clinical HDACi comparator mocetinostat or compound 5 in SGC-7901 cells. (B) Dose-dependent induction of cell cycle arrest by compound 5 in SGC-7901 cells at 24 h. (C) Induction of apoptosis at 48 h by compound 5 at 5 μM in SMMC-7721 cells. See Experimental Section for details.

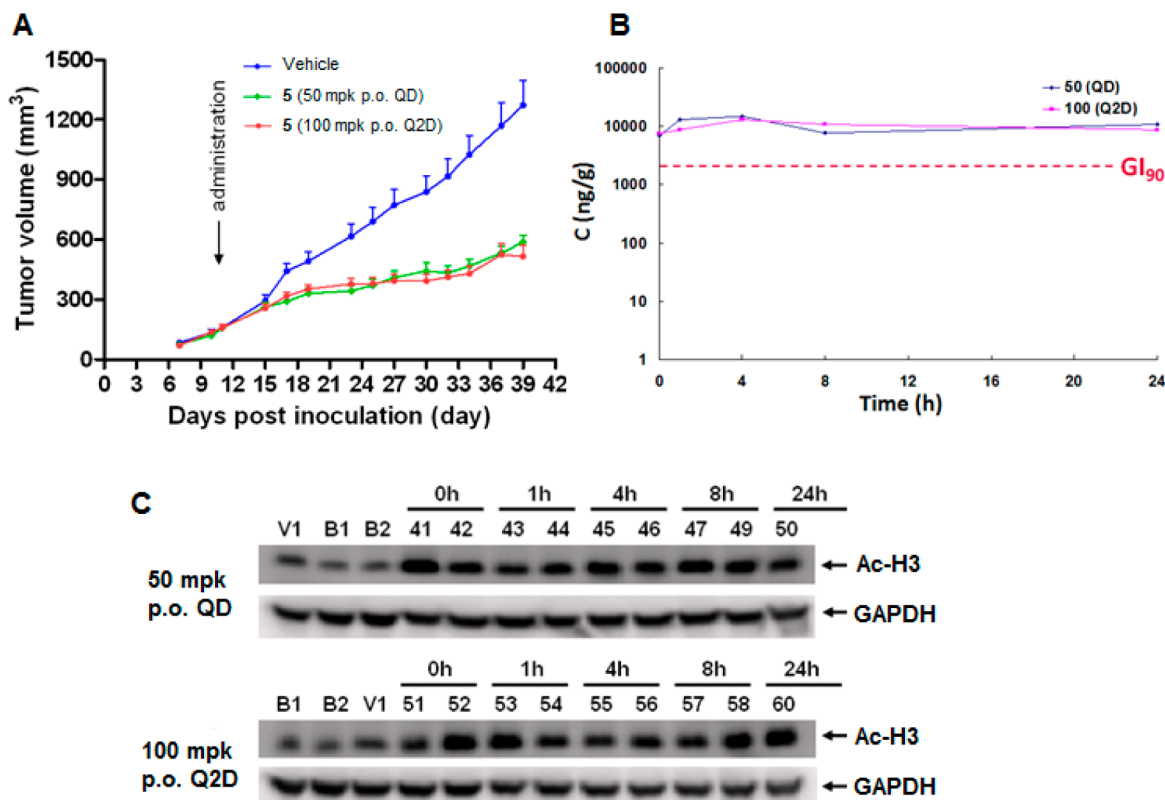


Figure 6. In vivo antitumor efficacy and PK/PD correlation for compound 5. (A) Effect of compound 5 on growth of an established BEL-7404 tumor in nude mice ($n = 9-10$) over four weeks. (B) Concentration of compound 5 in tumor tissue over 24 h period subsequent to the last dose. (C) Acetylated histone H3 induction in tumor tissue sampled at various time points after sacrificing mice subsequent to the last dose of compound 5.

assess response toward 5 and to identify candidate predictive biomarkers (see Supporting Information Table S5). Each model was treated with 5 at 100 mpk every other day (the efficacious dose in cell line-derived liver cancer xenografts) for approximately four weeks. In regards to biomarker hypothesis generation, while we recognized that global expression and methyl-ome profiling are ideal for unbiased biomarker discovery, practical considerations led us to choose instead the candidate gene approach for our pilot study. Thus, the

promoter CpG methylation status and mRNA expression level for 22 candidate genes (Table 7) were assessed on treatment days 0, 7, 15 and the last day of the study (see Supporting Information for more details on the study design) using Methyl-Profiler PCR arrays allowing for parallel analysis of up to 24 genes at a time (our rationale for the selection of these 22 candidate genes is detailed below). Histone-H3 acetylation and pharmacokinetic parameters were assessed by immunohisto-

Table 7. Twenty-Two Candidate Genes Evaluated as Potential Biomarkers for Tumor Response Prediction

candidate gene category description ^a	gene ID	function ^b	methylation frequency in HCC patients, ^c %	number of patients evaluated ^c	detected in microarray?	up-regulated by 5 in microarray?
TSGs methylated in patients; up-regulated by 5	CACNA1G	proliferation	20–40	85	Y	Y
	CCND2	cell cycle	60–80	26	Y	Y
	CDKN1C	cell cycle	20–40	20	Y	Y
	CDKN2B	cell cycle	40–60	301	Y	Y
	CTGF	adhesion	0–20	24	Y	Y
	FN1	adhesion	40–60	24	Y	Y
	SOCS1	apoptosis	60–80	250	Y	Y
	THBS1	adhesion	0–20	79	Y	Y
TSGs methylated in patients; not up-regulated by 5	TIMP3	invasion	20–40	238	Y	Y
	RASSF1	cell cycle	60–80	648	Y	N
	TFPI2	invasion	40–60	34	Y	N
	CDKN2A	cell cycle	40–60	1380	Y	N
TSGs methylated in patients; not detected in microarray	CDH1	adhesion	20–40	574	Y	N
	SPINT2	cell movement	80–100	26	N	N
	HIC1	cell cycle	80–100	67	N	N
up-regulated by 5; no patient methylation information available	PYCARD	apoptosis	20–40	36	N	N
	IGFBP3	apoptosis	not known	NA	Y	Y
	CEBPA	differentiation	not known	NA	Y	Y
	CDKN1A	cell cycle	not known	NA	Y	Y
oncogenes down-regulated by 5	SDC2	proliferation	not known	NA	Y	Y
	WNT5A	growth	not known	NA	Y	down-regulated
	CFLAR	apoptosis	not known	NA	Y	down-regulated

^aThe candidate genes were grouped into five categories according to their promoter CpG island methylation status in HCC patient tissues, their response to treatment with compound 5 in *in vitro* microarray studies, their detect-ability in our microarray studies, and their functional classification as tumor suppressor genes (TSGs) or oncogenes (OGs). ^bMicroarray data were analyzed by Ingenuity Pathway Analysis.²⁵ ^cInformation from PubMeth public database of promoter CpG methylation profiling in cancer tissues.²⁶

chemistry and compound 5 bioanalysis, respectively, on the last day of the study.

The 22 candidate genes were selected based upon the results of microarray gene expression profiling of 5 in liver cancer cell lines, qRT-PCR confirmation of treatment-responsive genes, and a public database of liver cancer tumor suppressor genes found to be methylated frequently in patients²⁶ (see Supporting Information for further details). Broadly, the candidate genes were grouped into five categories: (1) tumor suppressor genes (TSGs) with frequent CpG island promoter methylation in patient tissue and up-regulated by 5 in microarray profiling studies; (2) TSGs with frequent CpG island promoter methylation in patient tissue and not up-regulated by 5 in microarray profiling studies; (3) TSGs with frequent CpG island promoter methylation in patient tissue but not detected in microarray profiling studies due to low hybridization signal; (4) TSGs not known to be methylated in patient tissue but up-regulated by 5 in microarray profiling studies; (5) candidate oncogenes (OGs) down-regulated by 5 in microarray profiling studies (Table 7). We hypothesized that responsive tumors would have a qualitatively distinct epigenetic signature from nonresponsive tumors and that such a signature, if confirmed through functional studies and a larger tumor cohort, could potentially be used to select patients more likely to respond to treatment with 5.

Patient tumor models B and C demonstrated a significant response to 5 (~50% tumor growth inhibition) while patient tumor model A did not respond at all to compound treatment (Figure 7A). PK/PD analysis revealed that the tumor exposure

of 5 and the induction of acetylated histone H3 resulting from target engagement (as measured by immunohistochemistry over multiple time points) were somewhat lower in the nonresponding model (Figure 7B and 7C). This result suggests that the apparent lack of response toward 5 for model A may have been in part or in whole due to differences in compound exposure and target engagement in this model compared to the other two models.

Analysis of the CpG methylation status of the 22 candidate genes in the three primary tumor models revealed a significant difference in the methylation pattern between the responding models and the nonresponding model. In particular, in the responding models B and C, only one and two genes had CpG promoter methylation, respectively. In contrast, in the nonresponding model A, seven out of the twenty-two candidate genes were methylated (Table 8). These results suggest that the severity of baseline epigenetic silencing of these candidate (mostly tumor suppressor) genes may be predictive of tumor response to 5, or at least may contribute to the refractory nature of nonresponding model A. Hypothetically, if the nonresponsiveness of model A were functionally confirmed to be due to heavy promoter DNA methylation, then one potential approach to overcome this therapeutic resistance would be to treat patients with such heavy baseline methylation with a combination of HDAC and DNA methyltransferase inhibitors.²⁷

With regard to the ability of 5 to reactivate epigenetically silenced tumor suppressor genes, one hypermethylated TSG in one responder, SPINT2, was significantly up-regulated upon

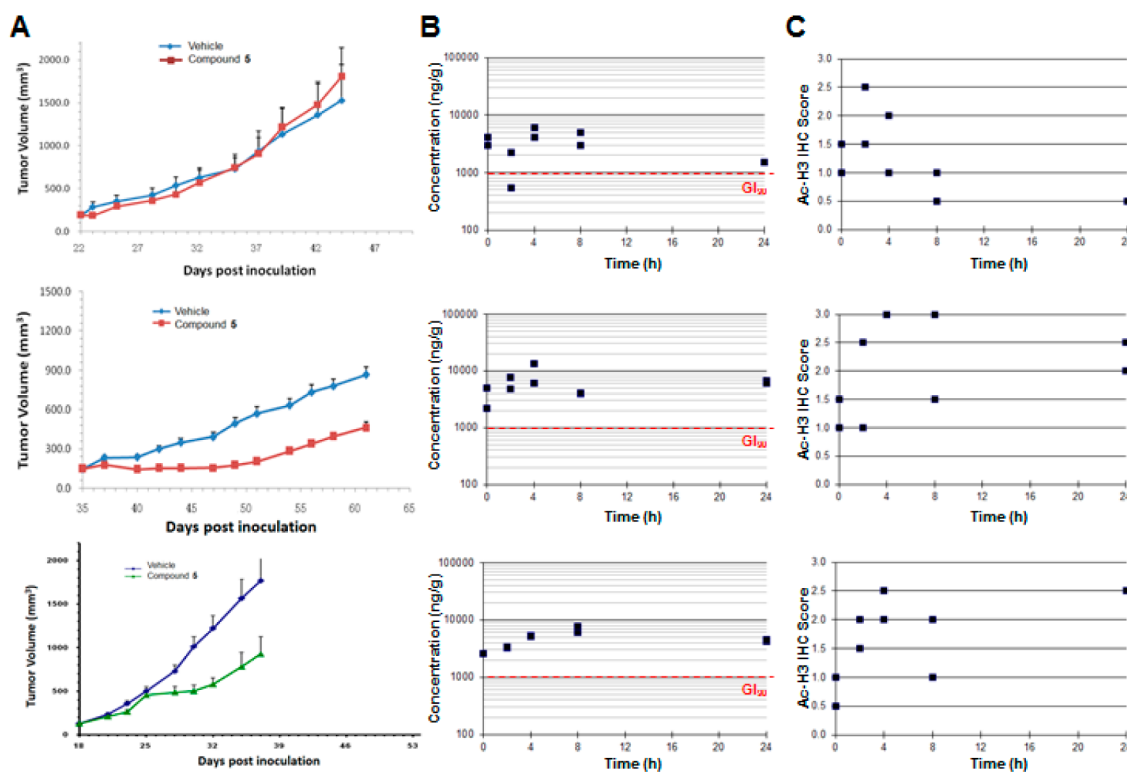


Figure 7. In vivo efficacy with PK/PD correlation for compound 5 in three patient tumor-derived xenograft models (top row = patient A; middle row = patient B; bottom row = patient C): (A) tumor growth curves for patients A–C treated with vehicle (15% Kleptose, pH 4.5 buffered with tartaric acid) or compound 5 Q2D PO 100 mpk. (B) Tumor concentration of compound 5 vs time for patients A–C (log 10 scale). Each square represents the concentration of 5 measured from a single mouse tumor. (C) Acetylated histone H3 IHC score (0–3) vs time for patients A–C (representative IHC sections scored as 0, 1, 2, or 3 available in Supporting Information Figure S6). Each square represents the IHC score from a single mouse tumor. See Experimental Section for further detail.

Table 8. Promoter CpG Island Methylation Status for Genes Methylated in at Least One out of Three Patients on Day 0, Start of Weeks 2 and 3, and Last Day of Study

gene ID ^a	patient A ^b	patient B ^b	patient C ^b
CACNA1G	X	–	–
CCND2	X	–	–
CDKN1C	X	–	–
SOCS1	X	–	–
RASSF1	X	X	X
TFPI2	X	–	–
SPINT2	X	–	X

^aOnly 7 out of 22 candidate genes are listed (the remaining 15 genes, CDKN2B, CTGF, FN1, THBS1, TIMP3, CDKNA2, CDH1, HIC1, PYCARD, IGFBP3, CEBPA, CDKN1A, SDC2, WNT5A, CFLAR, were not methylated in any of the three patients). ^b“X” = methylated as determined by methylation-specific PCR; “–” = not methylated as determined by methylation-specific PCR. Methylation status did not change over the course of the study. See Experimental Section for details.

treatment with 5. While a few other genes were up-regulated in both responding models at one or more time points (e.g., TIMP3, p21/CDKN1A), only the SPINT2 gene was both hypermethylated and responsive to treatment with 5 (Figure 8). Intriguingly, SPINT2 is an inhibitor of the HGF/MET pathway and has been identified as a TSG in certain cancers.²⁸ Future follow-up studies to these pilot experiments should evaluate the utility of SPINT2 as a potential biomarker in additional primary HCC tumor models as well as probe the

functional consequences of SPINT2 reactivation. Validation of the SPINT2 biomarker would suggest a rational means of selecting patients for combination therapy with 5 and MET kinase inhibitors.

In summary, the pilot epigenetic biomarker study of 5 in three primary liver cancer xenograft models indicated a potential correlation between baseline promoter methylation status of key tumor suppressor genes and tumor response, with heavy promoter methylation potentially predictive of poor response and suggesting combination therapy with DNA methyltransferase inhibitors. Furthermore, in one responder, a specific tumor suppressor gene with CpG island hypermethylation, SPINT2, was reactivated in response to compound treatment. The expression and promoter DNA methylation status of this gene deserves further assessment as a potential biomarker for response prediction and for combination therapy of 5 with MET kinase inhibitors. These preliminary findings should be interpreted in the context of the PK/PD data, which indicated somewhat lower compound 5 tumor exposure and target modulation for the nonresponding model.

CONCLUSION

Through a combination of scaffold hopping and structure–property relationship studies, we have developed an orally bioavailable HDAC inhibitor with selectivity toward the class I HDAC family and particular potency toward HDAC1. We demonstrated that this compound is more potent at inhibiting liver cancer cell growth in vitro as compared to clinical HDAC inhibitors entinostat and vorinostat and that its antiproliferative

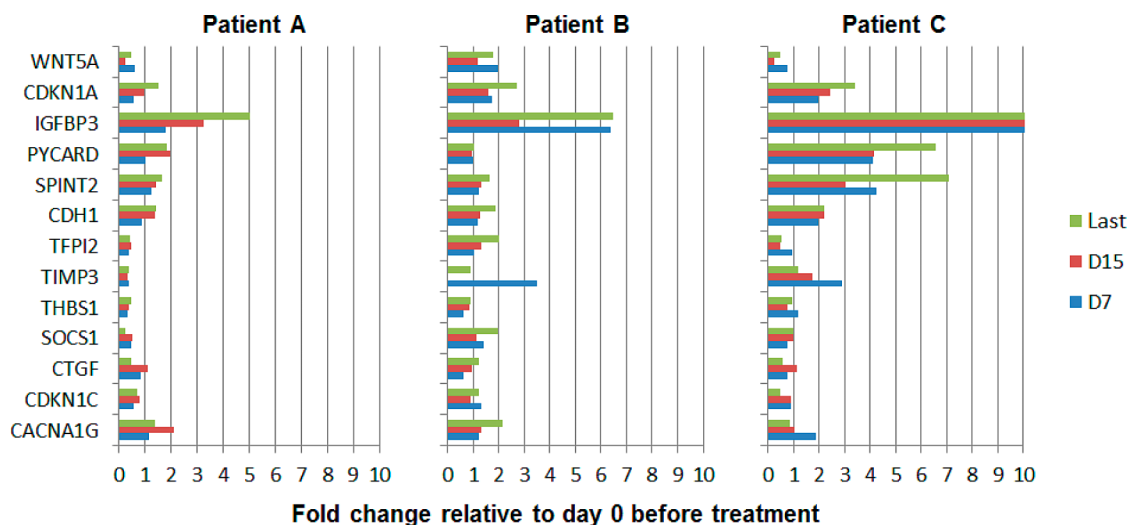


Figure 8. mRNA expression levels of candidate genes with absolute fold change greater than two at any of three time points (day 7, day 15, and last day of study) in the three patient models. CCND2, CDKN2B, FN1, RASSF1, CDKN2A, HIC1, CEBPA, SDC2, and CFLAR are not shown because these genes did not change significantly throughout the course of the experiment. Expression levels were determined by qRT-PCR, normalized to GAPDH, and reported as fold-change relative to day 0 (expression level before treatment). See Experimental Section for further details.

effects correlate to markers of in-cell target engagement such as acetylated histone H3 and p21/CDKN1A. Moreover, these in vitro effects translated into significant efficacy in both cell-based and patient tumor-derived xenograft models that appeared to correlate well to compound exposure levels and to changes in the same pharmacodynamic markers used to assess in-cell target engagement. One out of the three patient tumor models did not respond to treatment with our optimized HDAC inhibitor and, compared to the two responding models, had much higher levels of DNA methylation in the promoter regions of a panel of tumor suppressor genes known to be frequently epigenetically silenced in liver cancer patients. Furthermore, in one of the responding models, we identified SPINT2, an endogenous inhibitor of the progrowth HGF/MET pathway, as an epigenetically silenced gene whose expression could be reactivated by treatment with our HDAC inhibitor. Future research should seek to confirm the potential clinical utility of our candidate DNA methylation and tumor suppressor gene biomarkers in a larger cohort of patient tumor-derived models, through functional studies of these biomarkers, and in the context of combination therapy with either MET kinase inhibitors, DNA methyltransferase inhibitors, or the current standard of care in HCC, sorafenib.

EXPERIMENTAL SECTION

Molecular Docking. OPLS_2005 force field of MacroModel²⁹ was used to optimize the initial geometries of the compounds with a final root-mean-square gradient of 0.01 kcal/mol/Å. The default values of the optimization parameters and thresholds were retained. Glide XP was used for compound docking because of its robust energetic terms on metal–ligand interaction.³⁰ All torsion angles of compound were released to freely rotate, and 10000 docking runs were adopted during the XP docking with NE2 atom of His178 and zinc ion as docking constraints after trying different constraint combinations. Docking poses were clustered based on heavy atom RMSD values (1 Å), and top-ranked poses of each compound were selected and viewed graphically within the Maestro of Schrödinger program (Schrödinger, L.L.C., New York, NY), and finally displayed in Pymol (Schrödinger, L.L.C., New York, NY).

Microsomal Stability Assay. Each incubated mixture contained 0.5 mg/mL liver microsome (human or mouse), 100 mM potassium

phosphate buffer (pH = 7.4), 10 mM NADPH, and 1 μM of test compound in a total volume of 400 μL. After prewarming at 37 °C for 10 min, the NADPH was added to initiate the reaction. The reaction was terminated after 0, 3, 6, 9, 15, and 30 min by adding 150 μL of 100 ng/mL of tolbutamide (internal standard) in ice-cold methanol into 300 μL of incubation mixtures. Samples were then centrifuged at 4000 rpm for 10 min at 4 °C. The supernatant was then analyzed by LC-MS/MS.

Solubility Assay. DMSO stock solution (10 mM) of compound was prepared and divided into two portions. For one portion, the DMSO was evaporated to dryness and the remaining was redissolved in 50 mM phosphate buffer (pH 6.5). The mixture was stirred and shaken for 1 and 2 h, respectively. After the mixture was allowed to stand overnight, the solution was filtered before HPLC analysis. The other portion was used for the calibration curve preparation by diluting the DMSO stock solution using the same PBS buffer mentioned above to a series of solutions with concentration range of 50–500 μM.

Cytochrome P450 Inhibition Assay. A cocktail method that enables simultaneous incubation and measurement of compound inhibitory activity against CYP isoforms CYP3A4, CYP2D6, CYP2C9, CYP2C19, and CYP1A2 was developed with modification from previously reported methods.³¹ Each incubated mixture contained 0.125 mg/mL human liver microsome (protein content), 5 mM MgCl₂, 100 mM potassium phosphate buffer (pH = 7.4), substrate cocktail, various concentrations of test compound, and 2 mM NADPH in a total volume of 200 μL. The final concentrations of each CYP substrate were at the reported literature *K_m* values³¹ (see Supporting Information Table S2 for further details). Before addition of NADPH to initiate the reaction, mixtures were prewarmed at 37 °C for 10 min, and the reaction was terminated after 15 min of incubation by adding 100 μL of ice cold methanol containing 3 μM dextrorphan as an internal standard (IS). Samples were then centrifuged at 4000 rpm for 10 min at 4 °C. The supernatant was then analyzed by LC-MS/MS.

hERG Inhibition Assay. The inhibitory effect of compounds against the hERG channel was measured on an automated patch clamp system.³² CHO cells expressing hERG were loaded into the system. Cell solutions and buffer solutions were transferred to specially designed chips, where cells were attached to each well. Pressure changes were applied in each well until a gigaseal status and a whole cell configuration were achieved. After a brief stabilization process, a predefined pulse procedure was applied in each well, opening hERG channels and triggering tail currents. The peak of a tail current was measured. Compounds at various concentrations were then coincubated with the cell, and the same pulse procedure was repeated

to generate tail current data. Amoxicillin and amitriptyline were employed as negative and positive controls, respectively. Generally, a compound was tested at a minimum of two concentrations in duplicate, and thus IC_{20} or IC_{50} can be estimated to evaluate compound inhibitory potential on hERG channels.

PK Analyses. All compounds were evaluated in BALB/C nude mice (15–20 g, $N = 16$ per arm) except for compound **63** which was tested in male Sprague–Dawley rats (250 ± 20 g; $N = 3$). Compounds were administered by iv bolus at 2 mg/kg in 5% DMSO, 40% PEG400, and 55% saline and/or PO (gavage) at 10 mg/kg in 0.445% microcrystalline cellulose microsuspension. In each species, blood samples (150 μ L) were collected at eight time points (po) or nine time points (iv) into sodium heparin centrifuge tubes, and plasma samples were then isolated by centrifugation and stored at -20 °C prior to analysis. Plasma concentrations were determined by LCMS/MS and data were analyzed by noncompartmental methods using WinNonlin Pro (Pharsight Corp., Mountain View, CA).

Biology General Comments. Brief descriptions of the biological protocols used to generate data in this manuscript can be found below. For further details regarding experimental protocols, cell line origins, culture conditions, and reagent manufacturers, see Supporting Information.

HDAC Enzyme Inhibition Assay. HDAC enzyme inhibition assays were conducted by Reaction Biology Corporation as described (www.reactionbiology.com) using a 10-point dose response curve with half-log serial dilutions, fluorogenic peptide from p53 residues 379–382 (RHKKAc) at 50 μ M as substrate, and trichostatin A as a positive control.

p21 Reporter Gene Assay. Compounds were tested for their ability to induce p21 gene expression using a reporter gene assay involving HeLa cells transfected with a p21 promoter-luciferase construct. The p21 promoter contained the Sp1/Sp3 binding site for HDAC but not the upstream p53 binding site. Briefly, the day before transfection, HeLa cells were seeded at 11 000 cells/well in a 96-well culture plate and incubated at 37 °C in 5% CO_2 overnight. For transfection, the medium was removed and replaced with 100 μ L/well transfection media previously prepared as follows: 5 μ L of serum-free DMEM, 0.15 μ L of Fugene 6 reagent, 40 ng of p21-luc, 10 ng of GFP were mixed gently and incubated at room temperature for 30 min, and then 98 μ L of DMEM (with 10% FBS, 1% penicillin, and streptomycin) was added to the DNA:Fugene 6 reagent complex and mixed gently. After the cells were incubated for 24 h at 37 °C in 5% CO_2 , fresh media and test compounds were added to the wells and the cells further incubated for 15 h at 37 °C in 5% CO_2 . Cells were lysed by adding 80 μ L/well of a cell culture lysis reagent (Promega). A 50 μ L amount of each lysate was taken for GFP detection using an excitation wavelength of 486 nm and detection at 527 nm. A 100 μ L amount of Luciferase assay reagent (Promega) was then added to every 20 μ L of cell lysate for luminometer detection.

Cell Proliferation (water-soluble tetrazolium dye) Assay. Cells were seeded in 96-well culture plates (200 μ L/well at different seeding concentrations depending on cell type) and incubated overnight at 37 °C in 5% CO_2 . After adding compound dilutions (typically eight-point half-log serial dilutions in triplicate) to the cells (DMSO concentration kept below 0.5%), the cells were incubated at 37 °C in 5% CO_2 for 72 h. The effects on proliferation were determined by addition of CCK-8 reagent (Dojindo) according to the manufacturer's instruction, followed by incubation for 2 h at 37 °C in 5% CO_2 , and finally recording the absorbance at 450 nm using an ELISA plate reader.

Cell Cycle Analysis. An amount of 1×10^5 SGC-7901 cells was cultured overnight prior to treatment at about 50% confluency. Cells were treated with indicated concentrations of mocetinostat or **5** for 24 h. Cells were trypsinized and fixed with chilled 70% ethanol for 1 h at 4 °C. The cells were then resuspended in 500 μ L of propidium iodide (PI) solution (50 μ g/mL PI, 0.1 mg/mL RNase A and 0.05% Triton X-100) and incubated for 1 h at room temperature. Cells were washed three times with PBS and suspended in 500 μ L of PBS. PI positive cells were quantified using flow cytometer and CellQuest software (BD Biosciences).

Apoptosis Assay. An amount of 1×10^5 SMMC-7721 cells was treated with 5 μ M of mocetinostat or **5** for 48 h. Cells were trypsinized, washed twice with cold PBS, and then resuspended in 1X Annexin V binding buffer. A 100 μ L amount of the cell solution was incubated with 5 μ L of FITC/Annexin V for 15 min at room temperature. Cell samples were resuspended in 400 μ L of 1X Annexin V binding buffer, and FITC/Annexin V positive cells were quantified using flow cytometer and CellQuest software (BD Biosciences).

Western Blotting for p21 and Acetylated Histone H3 from Cells. An amount of 1×10^6 SGC-7901 cells was seeded overnight and then incubated with indicated concentrations of mocetinostat and **5** for 24 h. Cell extracts were prepared by lysing cultured cells into a mammalian protein extraction reagent supplemented with EDTA-free protease inhibitor on ice for 15 min. Supernatants were collected following centrifugation of lysed cells (15 000 g) for 10 min at 4 °C. For analysis of total cell lysates, 30 μ g of total protein per sample was resolved by SDS-PAGE and transferred onto nitrocellulose membrane. Membranes with immobilized proteins were probed with indicated antibodies. The reactive protein bands were visualized using enhanced chemiluminescence (ECL) detection system.

BEL-7404 Xenograft Efficacy Study. The use and care of experimental animals was approved by the Institutional Animal Care and Use Committee, Roche R&D Center (China). Female BALB/c nu/nu nude mice aged 6–7 weeks were obtained from Beijing Academy of Military Medical Science, Green violet blue Lab Animal Technology Co. Ltd. (Beijing, China), and housed in specific pathogen-free (SPF) conditions. Animals were held for a minimum of three days for acclimation prior to beginning the study. BEL-7404 suspended in serum-free RPMI-1640 (Invitrogen, Carlsbad, CA) was injected into the right flank of the nude mouse at 2.0×10^6 cells/mouse. After the tumor was established and reached 100–150 mm³, the mice were randomized into 10 mice per group and started to receive dosing of compound **5** (either QD PO 50 mpk or Q2D PO 100 mpk prepared in (15%) Kleptose-tartaric buffer (pH = 4.5)). The tumor growth was recorded three times a week from the measurement of length (L) and width (W) with caliper and calculated as tumor volume (TV, mm³) = $0.5 \times L \times W \times W$ (mm). The tumor growth inhibition (TGI) was calculated as $TGI\% = (1 - (\text{mean tumor volume of the treatment group on the first day} - \text{mean tumor volume of the treatment group on the end day}) / (\text{mean tumor volume of the control group on the first day} - \text{mean tumor volume of the control group on the end day})) \times 100\%$.

For PD biomarker evaluation, 50 mg of frozen tumor sample was dissected on dry ice and lysed in 500 μ L of tissue protein extraction reagent (Thermo Scientific) supplemented with EDTA-free protease inhibitors in MagNA lyser green beads and homogenized at 5000 rpm for 4×25 s (4 °C) using MagNA lyser (Roche). Tissue proteins were obtained from the supernatant of tissue homogenate by centrifugation at 15 000 rpm for 15 min (4 °C) and analyzed by Western blot (50 μ g of total protein per sample).

Patient Tumor-Derived Xenograft Model and PK/PD Analysis. The use and care of experimental animals was approved by the Institutional Animal Care and Use Committee, Roche R&D Center (China). Female BALB/c nu/nu nude mice aged 6–7 weeks were obtained from Shanghai SLAC Laboratory Animal Company (Shanghai, China) and housed in specific pathogen-free (SPF) conditions. The tumor fragments ($3 \times 3 \times 3$ mm³) derived from three HCC cancer patients were harvested for tumor inoculation. Under sterilized conditions, fragments were subcutaneously implanted into the right flank of nude mice for tumor development. Mice were randomized ($n = 10$ per dosing arm and 15 for biomarker satellite arm) and treatment initiated when tumors reached approximately 200 (150–250) mm³ as indicated (see Supporting Information for more study design details). Measurements were taken in the same way as in the BEL-7404 model study. Single-dose administration was also given as indicated on the last day of treatment, and the tumors were isolated at assigned time points (0 to 24 h postdosing) and cut into two pieces. The first piece from each tumor was subjected to pharmacokinetic analysis (see PK Analysis). The second piece from each tumor was subjected to immunohistochemistry. The 8 μ m paraffin embedded

tumor tissue slides were heated in a dry oven at 60 °C for 1 h and then deparaffinized and hydrolyzed by a Leica autostainer XL ST5010 at room temperature. Antigen retrieval was carried out at 95–99 °C in citrate buffer (0.01 M, pH 6.0) heated by a medical microwave at 92–98 °C for 5 min and then cooled to room temperature. Then peroxidase-blocking reagent (DAKO, DK-2600, Glostrup Denmark) was applied to quench the endogenous peroxidase. The slides were incubated in blocking serum for 20 min and then covered by 100 µL rabbit antihuman Ac-H3 (Lys9) antibody (Cell Signaling #9671, 1:200 in TBS/T) at 4 °C overnight. The slides were covered by 100 µL of DAKO Envision+ /HRP, rabbit/mouse after being washed thoroughly with TBS. One hundred microliters of substrate–chromogen solution (DAB) was applied to the slides and incubated at room temperature for 10 min. The slides were rinsed gently with tap water for 15 min. Counterstain and dehydration were performed with an XL ST5010 at room temperature. Finally, the slides were mounted with Permount mounting medium (Fisher Scientific, Miami, FL). The scoring was carried out by two pathologists independently (see Supporting Information for representative images and scores).

mRNA and Methylation Analysis by Real Time PCR. Human xenograft total RNA was extracted with TRIzol (Invitrogen), treated with DNAaseI (Promega), and further purified by RNA clean kit (Qiagen) before PCR. The 22-gene customized qRT-PCR array was designed by SABiosciences. Genomic DNA control, positive PCR control, and reverse transcription control were included in the array to monitor the PCR quality. GAPDH and β -glucuronidase were housekeeping genes used as internal controls. The reaction system and conditions were suggested by SABiosciences protocols. Bio-Rad Chromo4 was used for the qPCR reaction and detection. Amplification plots and dissociation curves were checked for reaction validity. Δ Ct values were calculated against the average of two housekeeping genes, and then the fold changes were calculated using lower expressed samples as control.

DNA methylation status was detected by using the customized “Methyl-Profiler” DNA methylation PCR array system (SABioscience). The experiments and analysis were performed by following the manufacturer’s manual. Briefly, the real time PCR primers for the 22 genes were designed, covering CpG islands in the DNA promoter regions. Four separate restriction enzyme digestion reactions were carried out to differentiate the methylation levels. Genomic DNA was extracted with a DNeasy kit (Qiagen) before the restriction digestions with the Methyl-Profiler enzyme kit (SABiosciences). The real-time PCR was performed under the suggested conditions from SABiosciences on a Bio-Rad Chromo4. The relative amount of each methylated DNA fraction is calculated using the standard Δ CT method, normalizing the amount of DNA in each digestion to the total amount of input DNA in the mock digestion. The quality control for the digestions was checked by the refractory DNA percentage during the analysis. Methylation superarray data were analyzed following Web site instructions (http://www.sabiosciences.com/dna_methylation_data_analysis.php).

Synthetic Chemistry General Comments. All starting materials were obtained commercially and were used without further purification. All reported yields are of isolated products and are not optimized. All final compounds were purified by preparative HPLC on a reverse phase column using Waters XBridge OBD Phenyl (30 × 100 mm, 5 µm) column or OBD RP18 (30 × 100 mm, 5 µm) column. LC/MS spectra were obtained using a MicroMass Platform LC (Waters alliance 2795-ZQ2000). For further details regarding preparative HPLC and LCMS protocols, see Supporting Information. NMR spectra were obtained using a Bruker AVANCE 400 MHz NMR spectrometer. All final compounds have purities greater than 95% based upon LC/MS and ¹H NMR. Enantiomeric excess was determined by chiral HPLC (see Supporting Information for details).

(2-Aminophenyl)carbamic Acid *tert*-Butyl Ester (II). To a solution of *o*-phenylenediamine (54.0 g, 0.500 mol) in THF (500 mL) was added (Boc)₂O (109 g, 0.500 mol) in THF (150 mL) dropwise, and the mixture was stirred at room temperature overnight. After concentration under vacuum, the residue was diluted with ethyl acetate/petroleum ether = 1/4 (v/v) (150 mL), and the precipitate

was collected. The mother liquor was concentrated, and the crude product was recrystallized with ethyl acetate/petroleum ether = 1/4 (v/v). The combined solids were dried in vacuo at 40 °C for 4 h. An off-white solid (80 g, 77%) was obtained. MS: calcd 209 (MH⁺), exp 209 (MH⁺). ¹H NMR (CDCl₃, 400 MHz) δ ppm 7.25 (m, 1H), 7.00 (m, 1H), 6.77 (m, 2H), 6.29 (broad m, 1H), 3.60 (broad m, 2H), 1.51 (s, 9H).

***N*-(2-(Acryloylamino)phenyl)carbamic Acid *tert*-Butyl Ester (III).** To a solution of acrylic acid (2.50 g, 34.7 mmol) in dichloromethane (80 mL) at 0 °C was added *N*-methylmorpholine (4.73 g, 46.8 mmol), followed by isobutyl chloroformate (6.37 g, 46.8 mmol). After 30 min, a solution of (2-aminophenyl)carbamic acid *tert*-butyl ester (II) (5.80 g, 27.8 mmol) in dichloromethane (50 mL) was added dropwise to the refluxing reaction mixture over 30 min. After the reaction was completed (2 h later), the reaction mixture was allowed to cool down to room temperature, poured into ice–water, and extracted with dichloromethane (30 mL × 3). The organic layer was washed with water, dilute sodium bicarbonate solution, 0.1 M HCl, water, and brine in turn. The organic layer was dried over sodium sulfate, filtered, and concentrated in vacuo. The crude solid was recrystallized from ethyl acetate/petroleum ether = 1/4 (v/v) to obtain the desired product (2.5 g, 34%). MS: calcd 263 (MH⁺), exp 263 (MH⁺). ¹H NMR (*d*₆-DMSO, 400 MHz) δ ppm 9.66 (s, 1 H), 8.45 (s, 1 H), 7.47 - 7.63 (m, 2 H), 7.03 - 7.23 (m, 2 H), 6.42 - 6.57 (m, 1 H), 6.27 (dd, *J* = 17, 2 Hz, 1 H), 5.79 (dd, *J* = 10, 2 Hz, 1 H), 1.46 (s, 9 H).

(*E*)-{4-[2-(2-*tert*-Butoxycarbonylamino)phenyl]phenyl}hydroxyacetic Acid Methyl Ester (IV). To a solution of (4-bromophenyl)hydroxyacetic acid (31.4 g, 136 mmol) in methanol (200 mL) was slowly added concentrated sulfuric acid (10 mL) dropwise, and then the reaction was heated to 50 °C for 3 h. The reaction was neutralized with sodium carbonate, concentrated by rotary evaporation, then extracted with ethyl acetate. Desired product I was recrystallized from hexanes/ethyl acetate (25.6 g, 77%) and used directly in the following step.

A mixture of *N*-(2-(acryloylamino)phenyl)carbamic acid *tert*-butyl ester (III) (23 g, 87.7 mmol), methyl-2-(4-bromophenyl)-2-hydroxyacetate (25.6 g, 104.5 mmol), tri-*o*-tolylphosphine (2.8 g, 9.2 mmol), Et₃N (35.8 g, 353.8 mmol), and Pd₂(dba)₃ (4.3 g, 4.7 mmol) in DMF (400 mL) was heated at 100 °C for 6 h under N₂ atmosphere and monitored by TLC. After being cooled to room temperature, the mixture was poured into a saturated aqueous solution of NH₄Cl and extracted with ethyl acetate. The organic layer was washed with brine, dried over Na₂SO₄, filtered, concentrated in vacuo, and purified by flash column chromatography (ethyl acetate/petroleum ether 1:2) to obtain pale yellow solid (IV) (22.4 g, 60%). MS: calcd 427 (MH⁺), exp 427 (MH⁺). ¹H NMR (DMSO-*d*₆, 400 MHz) δ ppm 9.71 (s, 1H), 8.48 (s, 1H), 7.64 (d, 2H, *J* = 8.0 Hz), 7.59 (d, 1H, *J* = 15.6 Hz), 7.57 (m, 1H), 7.48 (d, 2H, *J* = 8.0 Hz), 7.14 (m, 2H), 6.92 (d, 1H, *J* = 15.6, 6.17 (d, 1H, *J* = 5.2 Hz), 5.21 (d, 1H, *J* = 4.8 Hz), 3.64 (s, 3H), 1.47 (s, 9H).

(*E*)-{4-[2-(2-*tert*-Butoxycarbonylamino)phenyl]phenyl}hydroxyacetic Acid Methyl Ester (V). To a solution of {4-[2-(2-*tert*-butoxycarbonylamino)phenyl]phenyl}hydroxyacetic acid methyl ester (IV) (9.00 g, 21.1 mmol) and triethylamine (3.20 g, 31.6 mmol) in CH₂Cl₂ (135 mL) cooled to –5 °C was added dropwise methanesulfonyl chloride (3.14 g, 27.4 mmol) under N₂ atmosphere. The reaction was stirred at 0 °C until the starting material had been consumed according to TLC (about 1 h). The mixture was washed with water (90 mL) and brine (90 mL), dried with MgSO₄, filtered, and evaporated in vacuo to obtain 11.2 g (quantitative yield) of {4-[2-(2-*tert*-butoxycarbonylamino)phenyl]phenyl}methanesulfonyloxyacetic acid methyl ester as light yellow crystals which were used in the following step without further purification. MS: calcd 505 (MH⁺), exp 505 (MH⁺).

To a solution of {4-[2-(2-*tert*-butoxycarbonylamino)phenyl]phenyl}methanesulfonyloxyacetic acid methyl ester (1.26 g, 2.5 mmol) and Et₃N (0.76 g, 7.5 mmol) in CH₂Cl₂ (15 mL) was added (*S*)-3-hydroxypyrrolidine (0.27 g, 3 mmol). This mixture

was stirred overnight at room temperature, diluted with CH_2Cl_2 (50 mL), washed with saturated aqueous NaHCO_3 solution, water and brine, dried with Na_2SO_4 , filtered, and evaporated to obtain a yellow solid (V) which was directly used in the next reaction without further purification. MS: calcd 496 (MH⁺), exp 496 (MH⁺).

(E)-N-(2-Aminophenyl)-3-[4-[(4-bromophenylcarbamoyl)-(S)-3-hydroxypyrrolidin-1-yl)methyl]phenyl]acrylamide (3). To a solution of {4-[2-(2-*tert*-butoxycarbonylamino)phenylcarbamoyl]vinyl]phenyl}-(3-hydroxypyrrolidin-1-yl)acetic acid methyl ester (V) (1.23 g, 2.5 mmol) in MeOH (30 mL) was added aqueous LiOH (1 N, 10 mL). This mixture was stirred for about 5 h at room temperature and then evaporated to remove most of the MeOH. The aqueous layer was acidified with concentrated HCl to pH 5–6. The acidified aqueous layer was extracted with ethyl acetate (3 × 30 mL). The combined organic layer was washed with brine, dried with Na_2SO_4 , filtered, and evaporated to obtain 0.85 g (81%) of {4-[2-(2-*tert*-butoxycarbonylamino)phenylcarbamoyl]vinyl]phenyl}-(3-hydroxypyrrolidin-1-yl)acetic acid as a yellow solid product used directly in the following step. MS: calcd 482 (MH⁺), exp 482 (MH⁺).

To a solution of {4-[2-(2-*tert*-butoxycarbonylamino)phenylcarbamoyl]vinyl]phenyl}-(3-hydroxypyrrolidin-1-yl)acetic acid (2.3 g, 4.78 mmol), PyBrop (3 g, 6.4 mmol) and DIPEA (1 mL, 5.68 mmol) in CH_2Cl_2 (50 mL) was added 4-bromoaniline (1 g, 5.8 mmol). This mixture was stirred overnight at room temperature and then diluted with CH_2Cl_2 , washed with saturated aqueous NaHCO_3 solution, water, and brine, dried with Na_2SO_4 , and evaporated to obtain a yellow residue (VI). Hydrochloric acid in methanol (1.25 M, 30 mL) was added to the residue, the mixture was stirred for about 3 h, and then NaHCO_3 was added to the reaction system. After filtration of solids, the crude mixture was purified by preparative HPLC to obtain 520 mg of compound 3 as a pale-yellow solid (20%). MS: calcd 535 (MH⁺), exp 535 (MH⁺). ¹H NMR (MeOD-*d*₄, 400 MHz) δ ppm 7.83 (d, 2H, *J* = 8.0 Hz), 7.81 (d, 1H, *J* = 15.6 Hz), 7.75 (d, 2H, *J* = 8.0 Hz), 7.55 (d, 2H, *J* = 8.8 Hz), 7.49 (d, 2H, *J* = 8.8 Hz), 7.40–7.30 (m, 4H), 6.98 (d, 1H, *J* = 15.6 Hz), 5.24 (m, 1H), 4.60 (broad s, 1H), 4.00–3.80 (broad m, 2H), 3.60–3.20 (broad m, 2H), 2.35–2.15 (broad m, 2H).

***rac*-(*trans*-3,4)-4-(4-Bromophenyl)-1-methylpyrrolidine-3-carboxylic Acid Ethyl Ester (VII).** A mixture of sarcosine (44.5 g, 0.5 mol, 2.5 equiv), paraformaldehyde (60 g, 2 mol, 10 equiv), and (*E*)-3-(4-bromophenyl)acrylic acid ethyl ester (50 g, 196 mmol, 1 equiv) was heated under reflux in toluene (500 mL). The H_2O formed was removed with the aid of a Dean–Stark trap. After 4 h, the cooled mixture was filtered. The filtrate was concentrated. The residue was purified by chromatography on silica gel eluted with hexane–EtOAc to give 28 g of product (yield was 46%) and 26 g of starting material ethyl cinnamate (52%). MS: calcd (MH⁺) 312, exp (MH⁺) 312. ¹H NMR (CDCl_3 , 400 MHz) δ ppm 7.48 (d, 1H, *J* = 8.4 Hz), 7.29 (d, 2H, *J* = 8.4 Hz), 4.15 (q, 2H, 6.8 Hz), 3.51 (m, 1H), 3.30 (m, 2H), 3.20 (m, 2H), 2.72 (s, 3H), 1.21 (t, 3H, 6.8 Hz).

***rac*-(*trans*-3,4)-4-[4-[2-(2-*tert*-Butoxycarbonylamino)phenylcarbamoyl]vinyl]phenyl]-1-methylpyrrolidine-3-carboxylic Acid Ethyl Ester (VIII).** The mixture of compound *rac*-(*trans*-3,4)-4-(4-bromophenyl)-1-methylpyrrolidine-3-carboxylic acid ethyl ester (VII) (10.3 g, 33 mmol), *N*-(2-(acryloylamino)phenyl)carbamic acid *tert*-butyl ester (III) (9.51 g, 36.3 mmol), $\text{Pd}_2(\text{dba})_3$ (300 mg, 0.33 mmol), and *P*(*o*-tolyl)₃ (1.0 g, 3.3 mmol) in DMF (50 mL) and TEA (9 mL, 66 mmol) was stirred at 110 °C under N_2 in a sealed tube overnight. LC-MS indicated that the reaction was completed. The cooled mixture was partitioned between water and ethyl acetate. The organic phase was dried and concentrated. The residue was purified by chromatography on silica gel eluted by dichloromethane to give 14.22 g of desired product (87%). MS: calcd (MH⁺) 494, exp (MH⁺) 494.

***rac*-(*trans*-3,4)-4-[4-[2-(2-Aminophenylcarbamoyl)vinyl]phenyl]-1-methylpyrrolidine-3-carboxylic Acid (4-fluorophenyl)amide (12).** Lithium hydroxide monohydrate (2.42 g, 57.6 mmol) in water (20 mL) was added to a solution of *rac*-(*trans*-3,4)-4-[4-[2-(2-*tert*-butoxycarbonylamino)phenylcarbamoyl]vinyl]phenyl]-1-methylpyrrolidine-3-carboxylic acid ethyl ester (VIII) (14.22 g, 28.8 mmol) in methanol (80 mL). Then the mixture was stirred at room temperature overnight. LC-MS indicated that the

starting material was consumed. The mixture was adjusted to pH = 6–8 with 6 N HCl. The solvent was removed to give crude product *rac*-(*trans*-3,4)-4-[4-[2-(2-aminophenylcarbamoyl)vinyl]phenyl]-1-methylpyrrolidine-3-carboxylic acid which was used in the next step without further purification. ¹H NMR (CD_3OD , 400 MHz) δ ppm 7.81 (d, 1H, *J* = 15.6 Hz), 7.76 (d, 2H, *J* = 7.6 Hz), 7.70 (d, 1H, *J* = 7.6 Hz), 7.62 (d, 1H, *J* = 7.6 Hz), 7.58 (d, 2H, *J* = 8.0 Hz), 7.36 (t, 1H, *J* = 7.2 Hz), 7.29 (t, 1H, *J* = 7.2 Hz), 6.97 (d, 1H, *J* = 15.6 Hz), 4.02–3.84 (m, 2H), 3.82–3.64 (m, 2H), 3.33–3.26 (m, 2H), 3.12 (s, 3H), 1.63 (s, 9H).

HATU (13.3 g, 35 mmol) was added to a solution of compound *rac*-(*trans*-3,4)-4-[4-[2-(2-aminophenylcarbamoyl)vinyl]phenyl]-1-methylpyrrolidine-3-carboxylic acid (crude material, 28.8 mmol) and 4-fluorophenylamine (3.55 g, 32 mmol) in TEA (10 mL, 72 mmol), DMF (30 mL), and dichloromethane (300 mL) at rt. Then the mixture was stirred at rt for 3 h. LC-MS indicated that the reaction was completed. The mixture was partitioned between water and dichloromethane. The organic phase was dried and concentrated. The residue was purified by chromatography on silica gel to give 14.1 g of *rac*-[2-(3-[4-[(*trans*-3,4)-4-(4-fluorophenylcarbamoyl)-1-methylpyrrolidin-3-yl]phenyl]acryloylamino)phenyl]carbamic acid *tert*-butyl ester (88% over two steps). MS: calcd (MH⁺) 559, exp (MH⁺) 559.

rac-[2-(3-[4-[(*trans*-3,4)-4-(4-Fluorophenylcarbamoyl)-1-methylpyrrolidin-3-yl]phenyl]acryloylamino)phenyl]carbamic acid *tert*-butyl ester (14.5 g, 25.3 mmol) was dissolved in 150 mL of MeOH (with 1 N HCl) and stirred for 4 h. LC-MS indicated that the reaction was completed. The solvent was removed, and the residue was basified with TEA and purified by prep-HPLC to give 5 g of product 12 (43%). MS: calcd (MH⁺) 459, exp (MH⁺) 459. ¹H NMR (CD_3OD , 400 MHz) δ ppm 7.63–7.58 (m, 3H), 7.53–7.50 (m, 2H), 7.40 (d, 2H, *J* = 8.0 Hz), 7.21 (d, 1H, *J* = 7.6 Hz), 7.08–7.00 (m, 3H), 6.90–6.74 (m, 3H), 3.85 (m, 1H), 3.21–3.11 (m, 3H), 2.97–2.93 (m, 2H), 2.50 (s, 3H).

***rac*-(*trans*-3,4)-1-Benzyl-4-(4-bromophenyl)pyrrolidine-3-carboxylic Acid Ethyl Ester (IX).** To a mixture of ethyl *trans*-4-bromocinnamate (0.95 g, 3.73 mmol) and *N*-(methoxymethyl)-*N*-(trimethylsilylmethyl)benzylamine (1.06 g, 4.48 mmol) in dichloromethane (10 mL) was added orthoboric acid (23 mg, 0.37 mmol), and the mixture was stirred at room temperature for 2 days and heated at 45 °C for 2 h. The resulting mixture was concentrated in vacuo, and the crude product was purified by flash chromatography (PET:EtOAc = 10:1) to get product as colorless oil (1.08 g, 71%). MS: calcd 388 (MH⁺), exp 388 (MH⁺).

***rac*-(*trans*-3,4)-4-(4-Bromophenyl)pyrrolidine-3-carboxylic Acid Ethyl Ester (X).** To a solution of *rac*-(*trans*-3,4)-1-benzyl-4-(4-bromophenyl)pyrrolidine-3-carboxylic acid ethyl ester (IX) (3.97 g, 10.2 mmol) in acetonitrile (40 mL) was added K_2CO_3 (2.25 g, 16.3 mmol) followed by 2,2,2-trichloroethyl chloroformate (3.03 g, 14.3 mmol), and the mixture was heated at 60 °C for 3 h. The mixture was diluted with ethyl acetate and filtered. The filtrate was concentrated in vacuo, and the crude product was purified by flash chromatography (Pet:EtOAc = 10:1) to get *rac*-(*trans*-3,4)-4-(4-bromophenyl)pyrrolidine-1,3-dicarboxylic acid 3-ethyl ester 1-(2,2,2-trichloroethyl) ester as a colorless oil (3.2 g, 66.2%). MS: calcd 472 (MH⁺), exp 472 (MH⁺).

To a solution of *rac*-(*trans*-3,4)-4-(4-bromophenyl)pyrrolidine-1,3-dicarboxylic acid 3-ethyl ester 1-(2,2,2-trichloroethyl) ester (3.2 g, 6.76 mmol) in acetic acid (15 mL) was added Zn (1.28 g, 19.6 mmol) under Ar, and the mixture was stirred for 3 h at room temperature. The resulting mixture was diluted with dichloromethane and filtered. The filtrate was concentrated in vacuo. The crude product X (2.5 g) was obtained and used directly without further purification. MS: calcd 298 (MH⁺), exp (MH⁺) 298. ¹H NMR (CD_3OD , 400 MHz), 7.45 (d, 2H, *J* = 8.4 Hz), 7.21 (d, 2H, *J* = 8.4 Hz), 4.09 (t, 2H, *J* = 7.2 Hz), 3.47–3.33 (m, 3H), 3.26–3.21 (m, 1H), 3.09–3.05 (m, 1H), 2.89–2.84 (m, 1H), 1.16 (t, 3H, *J* = 7.2 Hz).

Representative Alkylation Procedure for R² Analogues of the 3,4-Disubstituted Pyrrolidine Series: *rac*-(*trans*-3,4)-4-(4-Bromophenyl)-1-(2-fluoroethyl)pyrrolidine-3-carboxylic Acid Ethyl Ester (XIa). A 20 mL microwave process vial was charged

with *rac*-(*trans*-3,4)-4-(4-bromophenyl)pyrrolidine-3-carboxylic acid ethyl ester (X) (1.49 g, 5 mmol), K₂CO₃ (1.38 g, 10 mmol), KI (41.5 mg, 0.25 mmol), and 1-bromo-2-fluoroethane (0.76 g, 6 mmol) in DMF (15 mL). The vial was sealed and heated at 130 °C for 20 min under microwave irradiation. After cooling, the solution was poured into water (30 mL), and the aqueous layer was extracted with ethyl acetate (3 × 50 mL). The combined organic layer was washed with brine, dried with Na₂SO₄, filtered, and evaporated. The crude product was purified by column chromatography (PE:EtOAc = 1:1) to give product as a yellow solid. MS: calcd 344 (MH⁺), exp 344 (MH⁺).

Representative Epoxidation Procedure for R² Analogues of the 3,4-Disubstituted Pyrrolidine Series: *rac*-(*trans*-3,4)-4-(4-Bromophenyl)-1-(2-hydroxy-2-methylpropyl)pyrrolidine-3-carboxylic Acid Ethyl Ester (XIb). To a solution of *rac*-(*trans*-3,4)-4-(4-bromophenyl)pyrrolidine-3-carboxylic acid ethyl ester (X) (5.0 g, 16.78 mmol) in ethanol (60 mL) was added 2,2-dimethyloxirane (8 mL). This mixture was heated for about 5 h at 80 °C in a sealed tube until the starting material had been consumed and then evaporated in vacuo to give 6.0 g (96%) of crude product as a yellow oil. MS: calcd 370 (MH⁺), exp 370 (MH⁺).

Representative Reductive Amination Procedure for R² Analogues of the 3,4-Disubstituted Pyrrolidine Series: *rac*-(*trans*-3,4)-4-(4-Bromophenyl)-1-isopropylpyrrolidine-3-carboxylic Acid Ethyl Ester (XIc). To a solution of *rac*-(*trans*-3,4)-4-(4-bromophenyl)pyrrolidine-3-carboxylic acid ethyl ester (X) (2.5 g, 8.39 mmol) in methanol were added acetone (9.73 g, 16.78 mmol), NaBH(OAc)₃ (3.56 g, 16.78 mmol), and catalytic acetic acid. This mixture was stirred at rt overnight until the starting material had been consumed. Water was added, and the organic phase was washed by brine, dried over Na₂SO₄, and concentrated to give 1.8 g of product (yield 64%). MS: calcd 340 (MH⁺), exp 340 (MH⁺).

Representative Acylation Procedure for R² Analogues of the 3,4-Disubstituted Pyrrolidine Series: *rac*-(*trans*-3,4)-4-(4-Bromophenyl)-1-ethylcarbamoylpyrrolidine-3-carboxylic Acid Ethyl Ester (XIId). To a solution of DIPEA (0.87 mL, 5 mmol) in dry THF was added triphosgene (530 mg, 1.8 mmol) at 0 °C, the resulting solution was stirred for 5 min, and then a solution of *rac*-(*trans*-3,4)-4-(4-bromophenyl)pyrrolidine-3-carboxylic acid ethyl ester (X) (1.485 g, 5 mmol) in THF and DIPEA (0.87 mL, 5 mmol) was added dropwise. After the mixture was stirring for an additional 20 min, ethylamine (450 mg, 10 mmol) was added dropwise and stirred overnight at room temperature before it was poured into H₂O (25 mL) and extracted with EtOAc (2 × 15 mL). The organic layer was washed with brine, dried over anhydrous Na₂SO₄, filtered, and concentrated in vacuo to give a crude product which was purified by flash column chromatography to yield the title compound (1.14 g, 62%) as a white solid. MS: calcd 369 (MH⁺), exp 369 (MH⁺).

Representative Nucleophilic Aromatic Substitution Procedure for R² Analogues of the 3,4-Disubstituted Pyrrolidine Series: *rac*-(*trans*-3,4)-4-[4-[(E)-2-(2-Aminophenylcarbamoyl)vinyl]phenyl]-1-pyrimidin-2-ylpyrrolidine-3-carboxylic Acid (4-Chlorophenyl)amide (XIe). To a solution of *rac*-(*trans*-3,4)-4-(4-bromophenyl)pyrrolidine-3-carboxylic acid ethyl ester (X) (466 mg, 1.56 mmol) in 2-propanol (6 mL) were added DIPEA (412 μL, 2.34 mmol) and 2-chloropyrimidine (228 mg, 2 mmol). The solution was heated to 130 °C for 10 min by microwave and then concentrated in vacuo and purified by flash chromatography to obtain 357 mg of product as an oil (60%). MS: calcd 376 (MH⁺), exp 376 (MH⁺).

***rac*-(*trans*-3,4)-4-[4-[2-(2-*tert*-Butoxycarbonylamino)phenylcarbamoyl]vinyl]phenyl]-1-(2-fluoroethyl)pyrrolidine-3-carboxylic Acid Ethyl Ester (XII).** To a solution of *rac*-(*trans*-3,4)-4-(4-bromophenyl)-1-(2-fluoroethyl)pyrrolidine-3-carboxylic acid ethyl ester (XIa) (2.0 g, 5.81 mmol), Pd₂(dba)₃ (265.8 mg, 0.29 mmol), tri-(*o*-tolyl)phosphine (88 mg, 0.29 mmol), and Et₃N (17.5 g, 17.4 mmol) in DMF (20 mL) was added *N*-(2-(acryloylamino)phenyl)-carbamoyl *tert*-butyl ester (III) (1.82 g, 6.97 mmol). This mixture was stirred at 100 °C for about 3 h until the starting material had been consumed, and then the reaction mixture was cooled and filtered. The solution was poured into water (40 mL) and extracted with ethyl acetate (3 × 60 mL). The combined organic layer was washed with brine, dried with Na₂SO₄, filtered, and evaporated. The crude product

was purified by column chromatography (PE:EtOAc = 1:1) to give yellow solid product. MS: calcd 526 (MH⁺), exp 526 (MH⁺).

***rac*-(*trans*-3,4)-4-[4-[2-(2-Aminophenylcarbamoyl)vinyl]phenyl]-1-(2-fluoroethyl)pyrrolidine-3-carboxylic Acid (4-chlorophenyl)amide (46).** To a solution of *rac*-(*trans*-3,4)-4-[4-[2-(2-*tert*-butoxycarbonylamino)phenylcarbamoyl]vinyl]phenyl]-1-(2-fluoroethyl)pyrrolidine-3-carboxylic acid ethyl ester (XII) (1.05 g, 2.0 mmol) in MeOH/H₂O (20 mL/6 mL) was added LiOH·H₂O (252 mg, 6.0 mmol). This mixture was stirred at room temperature overnight and then evaporated to remove most of the MeOH. The mixture was extracted with ethyl acetate (3 × 50 mL). The combined organic layer was washed with brine, dried with Na₂SO₄, filtered, and evaporated to get yellow solid product *rac*-(*trans*-3,4)-4-[4-[2-(2-*tert*-butoxycarbonylamino)phenylcarbamoyl]vinyl]phenyl]-1-(2-fluoroethyl)pyrrolidine-3-carboxylic acid. MS: calcd 498 (MH⁺), exp 498 (MH⁺).

To a solution of *rac*-(*trans*-3,4)-4-[4-[2-(2-*tert*-butoxycarbonylamino)phenylcarbamoyl]vinyl]phenyl]-1-(2-fluoroethyl)pyrrolidine-3-carboxylic acid (300 mg, 0.6 mmol), HATU (342 mg, 0.9 mmol), and Et₃N (181.8 mg, 1.8 mmol) in CH₂Cl₂ (15 mL) was added 4-chloroaniline (114.3 mg, 0.9 mmol). The reaction was stirred at room temperature overnight. The mixture was diluted with CH₂Cl₂ (15 mL), washed with water (15 mL) and brine (15 mL), dried with Na₂SO₄, filtered, and evaporated in vacuo to obtain light yellow residue which was used without further purification. MS: calcd 607 (MH⁺), exp 607 (MH⁺).

Hydrochloric acid in methanol (1.25 M, 5 mL) was added to the *rac*-[2-(3-{4-[(*trans*-3,4)-4-(4-chlorophenylcarbamoyl)-1-(2-fluoroethyl)pyrrolidin-3-yl]phenyl}acryloylamino)phenyl]carbamoyl *tert*-butyl ester residue, the mixture was stirred for about 3 h, and then NaHCO₃ was added to the reaction system. After filtration of solids, the crude mixture was purified by preparative HPLC to obtain light yellow solid. MS: calcd 507 (MH⁺), exp 507 (MH⁺). ¹H NMR (CD₃OD, 400 MHz), 7.66 (d, 1H, *J* = 15.6 Hz), 7.60 (d, 2H, *J* = 8.0 Hz), 7.53 (d, 2H, *J* = 8.8 Hz), 7.42 (d, 2H, *J* = 8.0 Hz), 7.21 (d, 1H, *J* = 8.0 Hz), 7.08–7.04 (m, 3H), 6.90–6.82 (m, 2H), 6.78–6.74 (m, 1H), 4.69 (t, 1H, *J* = 4.8 Hz), 4.57 (t, 1H, *J* = 4.8 Hz), 3.84–3.78 (m, 1H), 3.30–3.16 (m, 3H), 3.03–2.87 (m, 4H).

***rac*-(*trans*-3,4)-4-(4-Bromophenyl)pyrrolidine-1,3-dicarboxylic Acid 1-*tert*-Butyl Ester (XIII).** To a solution of *rac*-(*trans*-3,4)-4-(4-bromophenyl)pyrrolidine-3-carboxylic acid ethyl ester (X) (5.0 g, 16.8 mmol) in 20 mL of acetonitrile was added 20 mL of 2.5 M NaOH, and the resulted mixture was stirred at room temperature for 2 h. Then Na₂CO₃ (3.56 g 33.6 mmol) and Boc₂O (11 g, 50.4 mmol) were added, and the mixture was stirred at rt overnight. After removal of acetonitrile by vacuum, the residue was adjusted to pH 3. The solid was collected and triturated in hexane twice and dried by vacuum (50% yield). MS: calcd 370 (MH⁺), exp 370 (MH⁺).

***rac*-(*trans*-3,4)-3-(4-Bromophenyl)-4-(4-chlorophenylcarbamoyl)pyrrolidine-1-carboxylic Acid *tert*-Butyl Ester (XIV).** A suspension of *rac*-(*trans*-3,4)-4-(4-bromophenyl)pyrrolidine-1,3-dicarboxylic acid 1-*tert*-butyl ester (XIII) (3.1 g, 8.4 mmol), 4-chloroaniline (1.6 g, 12.6 mmol), HOBt (1.7 g, 12.6 mmol), and EDCI (2.4g, 12.6 mmol) in 50 mL of dichloromethane was stirred at rt overnight, and the reaction mixture was washed with 1 M NaOH, water, and brine. The organic layer was dried over Na₂SO₄ and concentrated to give yellow oil, which was used directly in the next step without purification. MS: calcd 479 (MH⁺), exp 479 (MH⁺).

***rac*-(*trans*-3,4)-4-(4-Bromophenyl)-1-(2-hydroxy-1,1-dimethylethyl)pyrrolidine-3-carboxylic Acid (4-Chlorophenyl)amide (XV).** *rac*-(*trans*-3,4)-3-(4-Bromophenyl)-4-(4-chlorophenylcarbamoyl)pyrrolidine-1-carboxylic acid *tert*-butyl ester (XIV) was dissolved in 15 mL of HCl/MeOH (1.25 M) and stirred at rt for 3 h. The reaction mixture was treated with saturated Na₂CO₃ solution and was extracted with dichloromethane. The organic layer was concentrated to give yellow oil, which was used without further purification. MS: calcd 379 (MH⁺), exp 379 (MH⁺).

To a solution of *rac*-(*trans*-3,4)-4-(4-bromophenyl)pyrrolidine-3-carboxylic acid (4-chlorophenyl)amide (1.12 g, 2.98 mmol) in 5 mL of

DMF were added K_2CO_3 (1.24 g, 8.9 mmol) and 2-bromo-2-methylpropionic acid methyl ester (0.81 g, 4.47 mmol), and the mixture was heated at 50 °C for 5 h. The reaction mixture was diluted with water and extracted with EtOAc, and the organic layer was washed with water and brine. After removal of solvent, the residue was dissolved in 30 mL of dry THF under N_2 atmosphere, and then $LiBH_4$ (2 M in THF, 2.9 mL, 5.8 mmol) was added dropwise at room temperature over 5 min. The resulting mixture was kept at this temperature for 2 h and then quenched by adding water carefully. The mixture was extracted with EtOAc, and the crude product was purified by column chromatography. A 0.23 g amount of product **XV** was obtained with a yield of 17%. MS: calcd 451 (MH⁺), exp 451 (MH⁺).

rac-(trans-3,4)-4-{4-[2-(2-Aminophenylcarbamoyl)vinyl]phenyl}-1-(2-hydroxy-1,1-dimethylethyl)pyrrolidine-3-carboxylic Acid (4-Chlorophenyl)amide (53). The mixture of *rac*-(trans-3,4)-4-(4-bromophenyl)-1-(2-hydroxy-1,1-dimethylethyl)pyrrolidine-3-carboxylic acid (4-chlorophenyl)amide (0.23 g, 0.5 mmol) (**XV**), *N*-(2-(acryloylamino)phenyl)carbamic acid *tert*-butyl ester *tert*-butyl ester (**III**) (0.14 g, 0.53 mmol), $Pd_2(dba)_3$ (37 mg, 0.04 mmol), and tri-(*o*-tolyl)phosphine (27 mg, 0.08 mmol) in DMF (3 mL) and TEA (0.35 mL, 2.5 mmol) was stirred at 100 °C under N_2 in a sealed tube for 3 h. The cooled mixture was partitioned between water and ethyl acetate. The organic phase was washed with water and brine, dried over Na_2SO_4 , and concentrated to give crude yellow oil. The crude oil was dissolved in 3 mL of HCl/MeOH (1.25 M) and stirred at room temperature for 3 h. The resultant mixture was neutralized with NH_3 /EtOH solution and purified by prep-HPLC to obtain 66 mg yellow solid as product. Yield was 24% over two steps. MS: calcd 533 (MH⁺), exp 533 (MH⁺). ¹H NMR (DMSO-*d*₆, 400 MHz), 10.09 (s, 1H), 9.36 (s, 1H), 7.50–7.61 (m, 5H), 7.33–7.39 (m, 5H), 6.84–6.94 (m, 2H), 6.75 (d, 1H, *J* = 8.0 Hz), 6.58 (t, 1H, *J* = 7.2 Hz), 4.93 (s, 2H), 4.46 (s, 1H), 3.62 (q, 1H, *J* = 7.6 Hz), 3.30 (m, 2H), 3.21–3.29 (m, 2H), 3.04 (q, 1H, *J* = 7.6 Hz), 2.78–2.88 (m, 2H), 1.03 (s, 3H), 1.01 (s, 3H).

rac-(trans-3,4)-4-(4-Bromophenyl)-1-tert-butylpyrrolidine-3-carboxylic Acid Ethyl Ester (XVI). A mixture of *N*-*tert*-butylglycine hydrochloride salt (0.9 g, 6.8 mmol), paraformaldehyde (1.5 g, 50 mmol), and ethyl cinnamate (0.9 g, 35 mmol) was heated under reflux in toluene (30 mL). The H_2O formed was removed with the aid of a Dean–Stark trap. After 4 h, the cooled mixture was filtered. The filtrate was concentrated. The residue was purified by chromatography on silica gel eluted with hexane–EtOAc to give 300 mg of product (yield was 12%). MS: calcd 354 (MH⁺), exp 354 (MH⁺).

rac-(trans-3,4)-4-{4-[2-(2-tert-Butoxycarbonylamino)phenylcarbamoyl]vinyl]phenyl}-1-tert-butylpyrrolidine-3-carboxylic Acid Ethyl Ester (XVII). A mixture of **XVI** (0.5 g, 1.4 mmol), *N*-(2-(acryloylamino)phenyl)carbamic acid *tert*-butyl ester (**III**) (0.5 g, 1.9 mmol), $Pd_2(dba)_3$ (100 mg, 0.01 mmol), and *P*(*o*-tolyl)₃ (100 mg, 0.33 mmol) in DMF (5 mL) and TEA (1 mL) was stirred at 110 °C under N_2 in a sealed tube overnight. LC-MS indicated that the reaction was completed. The cooled mixture was partitioned between water and ethyl acetate. The organic phase was dried and concentrated. The residue was purified by chromatography on silica gel eluted by dichloromethane to give 0.4 g of product (yield was 53%). MS: calcd 536 (MH⁺), exp 536 (MH⁺).

rac-(trans-3,4)-4-{4-[2-(2-Aminophenylcarbamoyl)vinyl]phenyl}-1-tert-butylpyrrolidine-3-carboxylic Acid (4-Chlorophenyl)amide (52). A solution of lithium hydroxide monohydrate (2.1 g, 50 mmol) in water (50 mL) was added to a solution of *rac*-(trans-3,4)-4-{4-[2-(2-tert-butoxycarbonylamino)phenylcarbamoyl]vinyl]phenyl}-1-tert-butylpyrrolidine-3-carboxylic acid ethyl ester (**XVII**) (0.4 g, 0.74 mmol) in THF (50 mL), and the mixture was stirred at room temperature overnight. LC-MS indicated that the starting material was consumed. The mixture was adjusted to pH = 6–8 with 6 N HCl. The solvent was removed to give crude *rac*-(trans-3,4)-4-{4-[2-(2-tert-butoxycarbonylamino)phenylcarbamoyl]vinyl]phenyl}-1-tert-butylpyrrolidine-3-carboxylic acid, which was used in the next step without further purification. MS: calcd 508 (MH⁺), exp 508 (MH⁺).

HATU (0.2 g, 0.52 mmol) was added to a solution of *rac*-(trans-3,4)-4-{4-[2-(2-tert-butoxycarbonylamino)phenylcarbamoyl]vinyl}-

phenyl]-1-*tert*-butylpyrrolidine-3-carboxylic acid (crude material, 0.2 mmol) and 4-chloroaniline (0.1 g, 0.78 mmol) in TEA (0.1 mL), and dichloromethane (7 mL) at rt, and the mixture was stirred at rt overnight. LC-MS indicated that the reaction was completed. The mixture was partitioned between water and dichloromethane. The organic phase was dried and concentrated. The residue was purified by chromatography on silica gel to give 80 mg of *rac*-[2-(3-{4-[(*trans*-3,4)-1-*tert*-butyl-4-(4-chlorophenylcarbamoyl)pyrrolidin-3-yl]phenyl]-acryloylamino)phenyl]carbamic acid *tert*-butyl ester (yield was 66%). MS: calcd 617 (MH⁺), exp 617 (MH⁺).

rac-[2-(3-{4-[(*trans*-3,4)-1-*tert*-Butyl-4-(4-chlorophenylcarbamoyl)pyrrolidin-3-yl]phenyl]acryloylamino)phenyl]carbamic acid *tert*-butyl ester (80 mg, 0.13 mmol) was dissolved in MeOH (1.25 M HCl, 10 mL) and stirred for 4 h. LC-MS indicated that the reaction was completed. The solvent was removed, and the residue was basified with TEA and purified by prep-HPLC to give 18 mg of product. MS: calcd (MH⁺) 517, exp (MH⁺) 517. ¹H NMR (CD₃OD, 400 MHz), 7.64 (d, 1H, *J* = 15.4 Hz), 7.55 (d, 2H, *J* = 8.0 Hz), 7.48 (d, 2H, *J* = 8.8 Hz), 7.39 (d, 2H, *J* = 8.0 Hz), 7.25 (d, 2H, *J* = 8.8 Hz), 7.19 (d, 1H, *J* = 8.0 Hz), 7.04 (t, 1H, *J* = 7.2 Hz), 6.87 (d, 1H, *J* = 8.0 Hz), 6.82 (d, 1H, *J* = 15.6 Hz), 6.74 (t, 1H, *J* = 7.6 Hz), 3.72 (m, 1H), 3.18–3.07 (m, 3H), 2.91 (m, 2H), 1.16 (s, 9H).

rac-(trans-3,4)-4-(4-Bromophenyl)-1-(2,2,2-trifluoroethyl)pyrrolidine-3-carboxylic Acid Ethyl Ester (XVIII). To a suspension of *rac*-(trans-3,4)-4-(4-bromophenyl)pyrrolidine-3-carboxylic acid ethyl ester hydrochloride (**X**) (1.10 g, 3.28 mmol) in DCM (10 mL) was added Et₃N (1.4 mL, 9.86 mmol). This mixture was stirred for about 5 min at room temperature and then cooled to 0 °C. To the resulting mixture was added trifluoroacetate anhydride (0.9 g, 4.28 mmol). The mixture was stirred for 30 min at 0 °C, warmed to room temperature, and stirred for 1 h. The resulting mixture was washed with water and brine, dried over Na_2SO_4 , filtered, and concentrated in vacuo. The crude product was purified by flash chromatography (Pet:EtOAc = 10:1) to get *rac*-(trans-3,4)-4-(4-bromophenyl)-1-(2,2,2-trifluoroacetyl)pyrrolidine-3-carboxylic acid ethyl ester as a colorless oil product (0.88 g, 68.1%).

To a solution of *rac*-(trans-3,4)-4-(4-bromophenyl)-1-(2,2,2-trifluoroacetyl)pyrrolidine-3-carboxylic acid ethyl ester (0.82 g, 2.08 mmol) was added a solution of borane in THF (3.3 mL, 3.3 mmol) at 0 °C. Then the mixture was refluxed for 2 h. The resulting mixture was cooled and quenched by aqueous HCl (6 N). The mixture was concentrated in vacuo to remove THF. The residue was basified by solid Na_2CO_3 and then extracted with EtOAc. The organic layer was washed with brine, dried with Na_2SO_4 , and concentrated in vacuo. The crude product was purified by flash chromatography (Pet:EtOAc = 20:1) to get colorless oil product **XVIII** (230 mg, 30%); 188 mg of starting material was recovered. MS: calcd 380 (MH⁺), exp 380 (MH⁺). ¹H NMR (CDCl₃, 400 MHz), 7.45 (d, 2H, *J* = 8.4 Hz), 7.23 (d, 2H, *J* = 8.4 Hz), 4.13–4.19 (m, 2H), 3.61–3.66 (m, 1H), 3.34–3.37 (m, 1H), 3.04–3.24 (m, 6H), 1.24 (t, 3H, *J* = 6.8 Hz).

rac-(trans-3,4)-4-(4-Bromophenyl)-1-(2,2,2-trifluoroethyl)pyrrolidine-3-carboxylic Acid (4-Chlorophenyl)amide (XIX). To a solution of *rac*-(trans-3,4)-4-(4-bromophenyl)-1-(2,2,2-trifluoroethyl)pyrrolidine-3-carboxylic acid ethyl ester (440 mg, 1.16 mmol) in methanol (3 mL) was added aqueous NaOH (2.9 mL, 2 M). The mixture was stirred at rt for 4 h. Then the mixture was concentrated in vacuo to remove methanol, and the residue was acidified by aqueous HCl and lyophilized to offer a colorless solid. MS: calcd 352 (MH⁺), exp 352 (MH⁺), calcd 350 (M – H), exp 350 (M – H).

To a suspension of the crude acid in DCM (10 mL) were added PyBrop (811 mg, 1.74 mmol), 4-chlorophenylamine (177 mg, 1.39 mmol), and DIPEA (0.5 mL, 2.84 mmol). The reaction was stirred at room temperature overnight and diluted with CH_2Cl_2 (10 mL). The mixture was washed with water (10 mL) and brine (10 mL), dried with Na_2SO_4 , filtered, and concentrated in vacuo. The crude product was purified by flash chromatography on silica gel (Pet:EtOAc = 5:1–2:1) to get the product (483 mg, 90%). MS: calcd 461 (MH⁺), exp 461 (MH⁺).

***rac*-(*trans*-3,4)-4-[4-[2-(2-Aminophenylcarbamoyl)vinyl]phenyl]-1-(2,2,2-trifluoroethyl)pyrrolidine-3-carboxylic Acid (4-Chlorophenyl)amide (48).** The mixture of *rac*-(*trans*-3,4)-4-(4-bromophenyl)-1-(2,2,2-trifluoroethyl)pyrrolidine-3-carboxylic acid (4-chlorophenyl)amide (XIX) (483 mg, 1.05 mmol), *N*-(2-(acryloylamino)phenyl)carbamic acid *tert*-butyl ester (302 mg, 1.15 mmol), Pd₂(dba)₃ (28.8 mg, 0.03 mmol), and P(*o*-tolyl)₃ (38.4 mg, 0.12 mmol) in DMF (50 mL) and TEA (0.42 mL, 3 mmol) was heated at 110 °C under Ar in a sealed tube for 4 h. The cooled mixture was concentrated in vacuo to remove DMF. The residue was purified by chromatography on silica gel (DCM:methanol = 40:1–20:1) to give *rac*-[2-(3-{4-[(*trans*-3,4)-4-(4-chlorophenylcarbamoyl)-1-(2,2,2-trifluoroethyl)pyrrolidin-3-yl]phenyl}acryloylamino)phenyl]carbamic acid *tert*-butyl ester (580 mg, 86%). MS: calcd 643(MH⁺), exp 643 (MH⁺).

To a solution of *rac*-[2-(3-{4-[(*trans*-3,4)-4-(4-chlorophenylcarbamoyl)-1-(2,2,2-trifluoroethyl)pyrrolidin-3-yl]phenyl}acryloylamino)phenyl]carbamic acid *tert*-butyl ester (580 mg, 0.9 mmol) in DCM (6 mL) was added trifluoroacetic acid (2 mL), and the mixture was stirred for 2 h. The solvent was removed, and the residue was basified with TEA and purified by prep-HPLC. MS: calcd 543 (MH⁺), exp 543 (MH⁺). ¹H NMR (CD₃OD, 400 MHz), 7.66 (d, 1H, *J* = 15.6 Hz), 7.60 (d, 2H, *J* = 8.0 Hz), 7.53 (d, 2H, *J* = 8.4 Hz), 7.42 (d, 2H, *J* = 8.0 Hz), 7.29 (d, 2H, *J* = 8.4 Hz), 7.21 (d, 1H, *J* = 7.6 Hz), 7.08–7.04 (m, 1H), 6.90–6.82 (m, 2H), 6.78–6.74 (m, 1H), 3.92–3.60 (m, 1H), 3.44–3.38 (m, 2H), 3.29–3.24 (m, 4H), 3.10–3.06 (m, 1H).

3-(5-Bromopyridin-2-yl)acrylic Acid Ethyl Ester (XX). To a solution of 5-bromo-2-iodopyridine (14.2 g, 50 mmol) in dry THF (160 mL) was added dropwise isopropyl magnesium chloride (30 mL, 60 mmol) at –20 °C under N₂. After the addition, the reaction mixture was stirred for about 2 h at the same temperature, and then DMF (5.11 g, 70 mmol) was added while keeping the temperature under 0 °C. The reaction temperature was allowed to rise to rt, the mixture was stirred for 1 h and quenched with saturated ammonium chloride (10 mL), and then the solution pH was adjusted to 7–8 with 2.0 M HCl. The solvent was removed and extracted with ethyl acetate (2 × 200 mL). The combined organic layer was washed with brine, dried with Na₂SO₄, filtered, and evaporated to obtain 8.5 g (90%) of 5-bromopyridine-2-carbaldehyde as a yellow solid product which was used directly in the next step without further purification. MS: calcd 186 (MH⁺), exp 186 (MH⁺).

To a solution of triethyl phosphonoacetate (10.2 g, 45.7 mmol), Et₃N (7 mL, 50.3 mmol), and lithium bromide (4.3 g, 50.3 mol) in CH₃CN (120 mL) was added 5-bromopyridine-2-carbaldehyde (8.5 g, 45.7 mmol). This mixture was stirred overnight at room temperature. When LC-MS indicated the reaction was complete, it was quenched with water (10 mL). Excess CH₃CN was removed in vacuo, and then the remaining mixture was extracted with EtOAc (2 × 100 mL). The combined organic layer was washed with brine, dried with Na₂SO₄, filtered, and evaporated. The crude product was purified by column chromatography (PE: EtOAc = 5:1) to give 7.8 g (67%) of a yellow solid product. MS: calcd 256 (MH⁺), exp 256 (MH⁺).

***rac*-(*trans*-3,4)-4-(5-Bromopyridin-2-yl)-1-methylpyrrolidine-3-carboxylic Acid Ethyl Ester (XXI).** To a solution of 3-(5-bromopyridin-2-yl)acrylic acid ethyl ester (XX) (3 g, 11.7 mmol) and paraformaldehyde (4.22 g, 140.4 mol) in toluene (200 mL) was added sarcosine (2.1 g, 23.4 mmol). This mixture was heated to reflux for 4 h, using Dean–Stark trap to remove the water formed in the reaction. LC-MS indicated that the reaction was complete. After cooling, the solution was filtered, and the solid was washed with EtOAc (2 × 50 mL). The combined organic layer was washed with water and brine, dried with Na₂SO₄, filtered, and evaporated. The crude product was purified by column chromatography (PE: EtOAc = 3:1) to give 2.8 g (77%) of a white solid product. MS: calcd 313 (MH⁺), exp 313 (MH⁺).

***rac*-(*trans*-3,4)-4-{5-[2-(2-Aminophenylcarbamoyl)vinyl]pyridin-2-yl}-1-methylpyrrolidine-3-carboxylic Acid (4-Chlorophenyl)amide (64).** To a solution of *rac*-(*trans*-3,4)-4-(5-bromopyridin-2-yl)-1-methylpyrrolidine-3-carboxylic acid ethyl ester (XXI) (2.1 g, 6.7 mmol) in dried DMF (50 mL) were added *N*-(2-

(acryloylamino)phenyl)carbamic acid *tert*-butyl ester (III) (2.1 g, 8.05 mmol), tris-*o*-tolylphosphine (0.41 g, 1.34 mmol), Pd₂(dba)₃ (0.62 g, 0.67 mmol), and Et₃N (2.7 g, 26.8 mmol). The resulting mixture was stirred for 3 h at 100 °C under argon. After cooling, the mixture was filtered, and the solvent was removed, diluted with EtOAc (100 mL), washed with water and brine, dried with Na₂SO₄, filtered, and evaporated to give an oil. The crude product was purified by column chromatography (PE: EtOAc = 1:1) to give 2.5 g (75%) of *rac*-(*trans*-3,4)-4-{5-[2-(2-*tert*-butoxycarbonylamino)phenylcarbamoyl]vinyl]pyridin-2-yl}-1-methylpyrrolidine-3-carboxylic acid ethyl ester as a white solid product. MS: calcd 495 (MH⁺), exp 495 (MH⁺).

To a solution of *rac*-(*trans*-3,4)-4-{5-[2-(2-*tert*-butoxycarbonylamino)phenylcarbamoyl]vinyl]pyridin-2-yl}-1-methylpyrrolidine-3-carboxylic acid ethyl ester (2.5 g, 5 mmol) in THF/H₂O (45 mL/15 mL) was added LiOH monohydrate (1.05 g, 25 mmol). This mixture was stirred for about 5 h at room temperature and then evaporated to remove most of the THF. The aqueous solution was acidified with 2 N HCl to pH 6–7 and then extracted with ethyl acetate (3 × 70 mL). The combined organic layer was washed with brine, dried with Na₂SO₄, filtered, and evaporated to obtain 2.0 g (85.6%) of *rac*-(*trans*-3,4)-4-{5-[2-(2-*tert*-butoxycarbonylamino)phenylcarbamoyl]vinyl]pyridin-2-yl}-1-methylpyrrolidine-3-carboxylic acid as a yellow solid product. MS: calcd 467 (MH⁺), exp 467 (MH⁺).

To a solution of *rac*-(*trans*-3,4)-4-{5-[2-(2-*tert*-butoxycarbonylamino)phenylcarbamoyl]vinyl]pyridin-2-yl}-1-methylpyrrolidine-3-carboxylic acid (350 mg, 0.75 mmol), 4-chloroaniline (115 mg, 0.9 mmol), and Et₃N (227 mg, 2.25 mol) in CH₂Cl₂ (50 mL) was added HATU (430 mg, 1.125 mmol). This mixture was stirred overnight at room temperature and then diluted with CH₂Cl₂ (50 mL), washed with saturated aqueous NaHCO₃ solution, water, and brine, dried with Na₂SO₄, and evaporated to obtain 0.23 g (53%) of *rac*-2-(3-{6-[(*trans*-3,4)-4-(4-chlorophenylcarbamoyl)-1-methylpyrrolidin-3-yl]pyridin-3-yl}acryloylamino)phenyl]carbamic acid *tert*-butyl ester as a yellow solid. MS: calcd 576 (MH⁺), exp 576 (MH⁺).

The solution of *rac*-2-(3-{6-[(*trans*-3,4)-4-(4-chlorophenylcarbamoyl)-1-methylpyrrolidin-3-yl]pyridin-3-yl}acryloylamino)phenyl]carbamic acid *tert*-butyl ester (168 mg, 0.3 mmol) in 2 N HCl in MeOH (10 mL) was stirred for 4 h at room temperature, and then the pH of the solution was adjusted to 8–9 with NaHCO₃ solution. Then the mixture was diluted with water (50 mL) and extracted with EtOAc (2 × 50 mL). The combined organic layer was washed with brine, dried with Na₂SO₄, filtered, and evaporated. The crude product was purified by preparative HPLC to give a yellow solid product. MS: calcd 476 (MH⁺), exp 476 (MH⁺). ¹H NMR (DMSO-*d*₆, 400 MHz), 10.16 (s, 1H), 9.44 (s, 1H), 8.76 (s, 1H), 7.97 (d, 1H *J* = 8.0 Hz), 7.63–7.56 (broad m, 3H), 7.41 (d, 1H, *J* = 8.4 Hz), 7.36–7.30 (broad m, 3H), 6.98–6.91 (broad m, 2H), 6.76 (d, 1H, *J* = 7.2 Hz), 6.58 (t, 1H, *J* = 7.2 Hz), 4.95 (broad s, 2H), 3.95 (m, 1H), 3.48 (m, 1H), 3.03 (broad m, 2H), 2.79 (m, 2H), 2.33 (s, 3H).

Ethyl 3-(2-[1,3]-Dioxolanpyridinyl)acrylate (XXII). To a solution of 5-bromopyridine-2-aldehyde (3.72 g, 20 mmol) in toluene (60 mL) were added TsOH monohydrate (190 mg, 1 mmol) and ethane-1,2-diol (2.48 g, 40 mmol). The mixture was heated to reflux for 6 h. The solvent was removed, and the residue was dissolved in ethyl acetate and washed with sodium bicarbonate and brine. The organic layer was dried with sodium sulfate and concentrated to give the crude product 5-bromo-2-[1,3]dioxolan-2-ylpyridine which was used in the next step without further purification. MS: calcd 230 (MH⁺), exp 230 (MH⁺).

To a solution of 5-bromo-2-[1,3]dioxolan-2-ylpyridine (460 mg, 2.0 mmol) in DMF (10 mL) were added ethyl acrylate (240 mg, 2.4 mmol), Pd₂(dba)₃ (183 mg, 0.2 mmol), tris-*o*-tolylphosphine (122 mg, 0.4 mmol), and Et₃N (606 mg, 6 mmol). The mixture was heated to 110 °C for 3 h under protection of nitrogen. The mixture was diluted with ethyl acetate and washed with brine. The organic layer was dried with sodium sulfate and concentrated. The residue was purified by chromatography to give the pure product. MS: calcd 250 (MH⁺), exp 250 (MH⁺).

***rac*-(*trans*-3,4)-4-(6-[1,3]dioxolan-2-ylpyridin-3-yl)-1-methylpyrrolidine-3-carboxylic Acid Ethyl Ester (XXIII).** To a solution of ethyl 3-{2-[1,3]-dioxolanpyridinyl}acrylate (6 g, 24 mmol) in toluene (600 mL) was added *N*-methylglycine (10.7 g, 120 mmol) and paraformaldehyde (14.4 g, 480 mmol). The mixture was heated to reflux for 6 h. After cooling, the solvent was removed and the residue was purified by chromatography to give the pure product. MS: calcd 307 (MH⁺), exp 307 (MH⁺).

***rac*-(*trans*-3,4)-4-[6-(2-*tert*-Butoxycarbonylvinyl)pyridin-3-yl]-1-methylpyrrolidine-3-carboxylic Acid Ethyl Ester (XXIV).** To a solution of *rac*-(*trans*-3,4)-4-(6-[1,3]dioxolan-2-ylpyridin-3-yl)-1-methylpyrrolidine-3-carboxylic acid ethyl ester (612 mg, 2 mmol) in DMSO/H₂O (12 mL/4 mL) was added LiCl (509 mg, 12 mmol). The mixture was sealed in a microwave tube and heated to 150 °C for 10 min under microwave conditions. The mixture was diluted with ethyl acetate and washed with brine. The organic layer was dried with sodium sulfate and concentrated. The residue was purified by chromatography to give the pure product *rac*-(*trans*-3,4)-4-(6-formylpyridin-3-yl)-1-methylpyrrolidine-3-carboxylic acid ethyl ester. MS: calcd 263 (MH⁺), exp 263 (MH⁺).

To the solution of *rac*-(*trans*-3,4)-4-(6-formylpyridin-3-yl)-1-methylpyrrolidine-3-carboxylic acid ethyl ester (1.31 g, 5 mmol) in THF (35 mL) was added diethyl *tert*-butyl phosphonoacetate (1.78 g, 7 mmol) at rt. *n*-Butyllithium (4 mL, 8 mmol) was added dropwise to the above solution at -78 °C. The solution was allowed to rise to 0 °C slowly and stirred at 0 °C for 2 h. The reaction was quenched with saturated ammonium chloride. The solvent was removed, and the residue was dissolved in ethyl acetate. The organic layer was washed with brine and dried with sodium sulfate. The solvent was concentrated, and the residue was purified by chromatography to give the pure product. MS: calcd 361 (MH⁺), exp 361 (MH⁺).

***rac*-3-{5-[(*trans*-3,4)-4-(4-Chlorophenylcarbamoyl)-1-methylpyrrolidin-3-yl]pyridin-2-yl}acrylic acid *tert*-Butyl Ester (XXV).** To a solution of *rac*-(*trans*-3,4)-4-[6-(2-*tert*-butoxycarbonylvinyl)pyridin-3-yl]-1-methylpyrrolidine-3-carboxylic acid ethyl ester (500 mg, 1.39 mmol) in THF (9 mL) was added lithium hydroxide monohydrate (234 mg, 5.56 mmol) and water (3 mL). The mixture was stirred at rt for 3 h. The solution was neutralized to pH 6–7. The solvent was removed, and the residue (*rac*-(*trans*-3,4)-4-[6-(2-*tert*-butoxycarbonylvinyl)pyridin-3-yl]-1-methylpyrrolidine-3-carboxylic acid) was used directly in the next step. MS: calcd 333 (MH⁺), exp 333 (MH⁺).

To a solution of *rac*-(*trans*-3,4)-4-[6-(2-*tert*-butoxycarbonylvinyl)pyridin-3-yl]-1-methylpyrrolidine-3-carboxylic acid (430 mg, 1.3 mmol) in dichloromethane (10 mL) were added HATU (990 mg, 2.6 mmol), Et₃N (525 mg, 5.2 mmol), and 4-chloroaniline (249 mg, 1.95 mmol). The mixture was stirred at rt for 24 h. The solvent was removed, and the residue was dissolved in ethyl acetate. The organic layer was washed with brine and dried with sodium sulfate. The solvent was removed, and the residue was purified by chromatography to give the pure product. MS: calcd 442 (MH⁺), exp 442 (MH⁺).

***rac*-(*trans*-3,4)-4-[6-[2-(2-Aminophenylcarbamoyl)vinyl]pyridin-3-yl]-1-methylpyrrolidine-3-carboxylic Acid (4-Chlorophenyl)amide (61).** To a solution of *rac*-3-{5-[(*trans*-3,4)-4-(4-chlorophenylcarbamoyl)-1-methylpyrrolidin-3-yl]pyridin-2-yl}acrylic acid *tert*-butyl ester (172 mg, 0.5 mmol) in dichloromethane (5 mL) was added trifluoroacetic acid (570 mg, 5 mmol) at 0 °C. The solution was allowed to rise to rt and stirred for 2 h. The solvent was removed under reduced pressure to give the crude product (*rac*-3-{5-[(*trans*-3,4)-4-(4-chlorophenylcarbamoyl)-1-methylpyrrolidin-3-yl]pyridin-2-yl}acrylic acid) which was used directly in next step. MS: calcd 386 (MH⁺), exp 386 (MH⁺).

To a solution of *rac*-3-{5-[(*trans*-3,4)-4-(4-chlorophenylcarbamoyl)-1-methylpyrrolidin-3-yl]pyridin-2-yl}acrylic acid (54 mg, 0.14 mmol) in dichloromethane (3 mL) were added 1,2-diaminobenzene (46 mg, 0.42 mmol), HATU (80 mg, 0.21 mmol), and Et₃N (85 mg, 0.84 mmol). The mixture was stirred at rt for 12 h. The solvent was removed, and the residue was dissolved in ethyl acetate. The solution was washed with brine and dried with sodium sulfate. The solvent was concentrated to give the residue, which was purified by preparative

HPLC to give pure product. MS: calcd 476 (MH⁺), exp 476 (MH⁺). ¹H NMR (CD₃OD, 400 MHz), 8.57 (s, 1H), 7.88 (d, 1H, *J* = 8.4 Hz), 7.68–7.62 (m, 2H), 7.53 (d, 2H, *J* = 8.8 Hz), 7.28 (d, 2H, *J* = 8.8 Hz), 7.22–7.18 (m, 2H), 7.05 (t, 1H, *J* = 7.6 Hz), 6.87 (d, 1H, *J* = 8.0 Hz), 6.76 (t, 1H, *J* = 7.6 Hz), 3.90 (q, 1H, *J* = 8.0 Hz), 3.32–3.18 (broad m, 3H), 3.01 (t, 2H, *J* = 8.4 Hz), 2.54 (s, 3H).

■ ASSOCIATED CONTENT

Supporting Information

Additional information regarding compound characterization (LCMS and ¹H NMR), supplemental SAR data, and experimental details for the CYP inhibition assay, metabolite identification, cell lines and biological reagents, patient-derived xenograft model study design, microarray profiling study of compound 5, and immunohistochemistry scoring images. This material is available free of charge via the Internet at <http://pubs.acs.org>.

■ AUTHOR INFORMATION

Corresponding Author

*Phone: 1-510-710-4129. E-mail: jwong@alum.mit.edu.

Present Address

#14 Moon Beam Drive, Mountain View, CA 94043.

Notes

The authors declare no competing financial interest.

■ ACKNOWLEDGMENTS

We thank members of the following departments of the Roche R&D Center (China) Ltd. for research support: (1) the department of analytical chemistry (Wenzhi Cheng, Lucy Lu, Sterling Yuan, Harkin Gao, Dr. Penny Ding, Dr. Fred Li) for support on purification and characterization of compounds; (2) the DMPK department (Hongxia Qiu, Yuxia Zhang, Jian Xin) for conducting microsome, solubility, and CYP inhibition studies; (3) the compound management and inventory group (Lana Liu, Bill Wang, Qinghong Lv, Dr. Lynn Lin) for support on obtaining and tracking synthetic reagents and formatting final compounds for biological assays.

■ ABBREVIATIONS USED

AFP, α -fetoprotein; AUC, area under curve; Boc, COOC-(CH₃)₃; CL, systemic clearance rate; CYP, cytochrome P450; dba, dibenzylideneacetone; DCM, dichloromethane; DIPEA, diisopropylethylamine; DMAP, 4-dimethylaminopyridine; DMF, dimethylformamide; DMPK, distribution, metabolism, pharmacokinetics; DMSO, dimethyl sulfoxide; EDCl, 1-ethyl-3-(3-dimethylaminopropyl)carbodiimide hydrochloride; EtOH, ethanol; F, bioavailability; GFP, green fluorescent protein; HATU, 1-[bis(dimethylamino)methylene]-1*H*-1,2,3-triazolo-[4,5-*b*]pyridinium hexafluorophosphate 3-oxide; HBV, hepatitis B virus; HCC, hepatocellular carcinoma; HDAC, histone deacetylase; HDACi, histone deacetylase inhibitor; hERG, human ether-à-go-go related gene; HLM, human liver microsomes; HOBt, hydroxybenzotriazole; HWE, Horner–Wadsworth–Emmons; IHC, immunohistochemistry; *i*-PrOH, 2-propanol; MeOH, methanol; MLM, mouse liver microsomes; mpk, milligrams per kilogram; Ms, mesyl; NAD, nicotinamide adenine dinucleotide; PD, pharmacodynamics; PE, petroleum ether; PK, pharmacokinetics; PO, oral administration; Q2D, once every two days; QD, every day; qRT-PCR, quantitative real time polymerase chain reaction; SAR, structure–activity relationship; SPR, structure–property relationship; TEA,

triethylamine; TFA, trifluoroacetic acid; THF, tetrahydrofuran; TSG, tumor suppressor gene; V_{ss} , volume of distribution at steady state; WST, water-soluble tetrazolium dye

REFERENCES

- (1) El-Seraq, H. B. Hepatocellular carcinoma. *N. Engl. J. Med.* **2011**, *365*, 1118–1127.
- (2) Bruix, J.; Llovet, J. M. Prognostic prediction and treatment strategy in hepatocellular carcinoma. *Hepatology* **2002**, *35*, 519–524.
- (3) Llovet, J. M.; Ricci, S.; Mazzaferro, V.; Hilgard, P.; Gane, E.; Blanc, J. F.; de Oliveira, A. C.; Santoro, A.; Raoul, J. L.; Forner, A.; Schwartz, M.; Porta, C.; Zeuzem, S.; Bolondi, L.; Gretten, T. F.; Galle, P. R.; Seitz, J. F.; Borbath, I.; Häussinger, D.; Giannaris, T.; Shan, M.; Moscovici, M.; Voliotis, D.; Bruix, J. Sorafenib in advanced hepatocellular carcinoma. *N. Engl. J. Med.* **2008**, *359*, 378–390.
- (4) Yang, X. J.; Seto, E. The Rpd3/Hda1 family of lysine deacetylases: from bacteria and yeast to mice and men. *Nat. Rev. Mol. Cell Biol.* **2008**, *9*, 206–218.
- (5) Grozinger, C. M.; Schreiber, S. L. Deacetylase enzymes: biological functions and the use of small-molecule inhibitors. *Chem. Biol.* **2002**, *9*, 3–16.
- (6) Rikimaru, T.; Taketomi, A.; Yamashita, Y.; Shirabe, K.; Hamatsu, T.; Shimada, M.; Maehara, Y. Clinical significance of histone deacetylase 1 expression in patients with hepatocellular carcinoma. *Oncology* **2007**, *72*, 69–74.
- (7) Yoo, Y. G.; Na, T. Y.; Seo, H. W.; Seong, J. K.; Park, C. K.; Shin, Y. K.; Lee, M. O. Hepatitis B virus X protein induces the expression of MTA1 and HDAC1, which enhances hypoxia signaling in hepatocellular carcinoma cells. *Oncogene* **2008**, *27*, 3405–3413.
- (8) Wang, H.; Guo, Y.; Fu, M.; Liang, X.; Zhang, X.; Wang, R.; Lin, C.; Qian, H. Antitumor activity of Chidamide in hepatocellular carcinoma cell lines. *Mol. Med. Rep.* **2012**, *5*, 1503–1508.
- (9) Ma, B. B.; Sung, F.; Tao, Q.; Poon, F. F.; Lui, V. W.; Yeo, W.; Chan, S. L.; Chan, A. T. The preclinical activity of the histone deacetylase inhibitor PXD101 (belinostat) in hepatocellular carcinoma cell lines. *Invest. New Drugs* **2010**, *28*, 107–114.
- (10) Zhang, C.; Li, H.; Zhou, G.; Zhang, Q.; Zhang, T.; Li, J.; Zhang, J.; Hou, J.; Liew, C. T.; Yin, D. Transcriptional silencing of the TMS1/ASC tumour suppressor gene by an epigenetic mechanism in hepatocellular carcinoma cells. *J. Pathol.* **2007**, *212*, 134–142.
- (11) Wong, C. M.; Ng, Y. L.; Lee, J. M.; Wong, C. C.; Cheung, O. F.; Chan, C. Y.; Tung, E. K.; Ching, Y. P.; Ng, I. O. Tissue factor pathway inhibitor-2 as a frequently silenced tumor suppressor gene in hepatocellular carcinoma. *Hepatology* **2007**, *45*, 1129–1138.
- (12) Baylin, S. B. DNA methylation and gene silencing in cancer. *Nat. Clin. Pract. Oncol.* **2005**, *2*, S4–S11.
- (13) Lu, Y. S.; Kashida, Y.; Kulp, S. K.; Wang, Y. C.; Wang, D.; Hung, J. H.; Tang, M.; Lin, Z. Z.; Chen, T. J.; Cheng, A. L.; Chen, C. S. Efficacy of a novel histone deacetylase inhibitor in murine models of hepatocellular carcinoma. *Hepatology* **2007**, *46*, 1119–1130.
- (14) See for example: clinical trials.gov identifiers NCT00823290, NCT00943449, and NCT00537121 at www.clinicaltrials.gov.
- (15) (a) Miller, T. A.; Witter, D. J.; Belvedere, S. Histone deacetylase inhibitors. *J. Med. Chem.* **2003**, *46*, 5097–5116. (b) Wong, J. C.; Hong, R.; Schreiber, S. L. Structural biasing elements for in-cell histone deacetylase paralog selectivity. *J. Am. Chem. Soc.* **2003**, *125*, 5586–5587. (c) Ning, Z. Q.; Li, Z. B.; Newman, M. J.; Shan, S.; Wang, X. H.; Pan, D. S.; Zhang, J.; Dong, M.; Du, X.; Lu, X. P. Chidamide (CS055/HBI-8000): a new histone deacetylase inhibitor of the benzamide class with antitumor activity and the ability to enhance immune cell-mediated tumor cell cytotoxicity. *Cancer Chemother. Pharmacol.* **2012**, *69*, 901–909.
- (16) Yap, T. A.; Sandhu, S. K.; Workman, P.; de Bono, J. S. Envisioning the future of early anticancer drug development. *Nat. Rev. Cancer* **2010**, *10*, 514–523.
- (17) Venugopal, B.; Evans, T. R. Developing histone deacetylase inhibitors as anti-cancer therapeutics. *Curr. Med. Chem.* **2011**, *18*, 1658–1671.
- (18) (a) Khan, O.; Fotheringham, S.; Wood, V.; Stimson, L.; Zhang, C.; Pezzella, F.; Duvic, M.; Kerr, D. J.; La Thangue, N. B. HR23B is a biomarker for tumor sensitivity to HDAC inhibitor-based therapy. *Proc. Natl. Acad. Sci. U.S.A.* **2010**, *107*, 6532–6537. (b) Miyanaga, A.; Gemma, A.; Noro, R.; Kataoka, K.; Matsuda, K.; Nara, M.; Okano, T.; Seike, M.; Yoshimura, A.; Kawakami, A.; Uesaka, H.; Nakae, H.; Kudoh, S. Antitumor activity of histone deacetylase inhibitors in non-small cell lung cancer cells: development of a molecular predictive model. *Mol. Cancer Ther.* **2008**, *7*, 1923–1930. (c) Dejligbjerg, M.; Grauslund, M.; Christensen, I. J.; Tjørnelund, J.; Buhl Jensen, P.; Sehested, M. Identification of predictive biomarkers for the histone deacetylase inhibitor belinostat in a panel of human cancer cell lines. *Cancer Biomark.* **2008**, *4*, 101–109. (d) Fantin, V. R.; Loboda, A.; Paweletz, C. P.; Hendrickson, R. C.; Pierce, J. W.; Roth, J. A.; Li, L.; Gooden, F.; Korenchuk, S.; Hou, X. S.; Harrington, E. A.; Randolph, S.; Reilly, J. F.; Ware, C. M.; Kadin, M. E.; Frankel, S. R.; Richon, V. M. Constitutive activation of signal transducers and activators of transcription predicts vorinostat resistance in cutaneous T-cell lymphoma. *Cancer Res.* **2008**, *68*, 3785–3794. (e) For a general review on the subject of HDACi and biomarkers, refer to: Stimson, L.; La Thangue, N. B. Biomarkers for predicting clinical responses to HDAC inhibitors. *Cancer Lett.* **2009**, *280*, 177–183.
- (19) Wong, J. C.; Guo, L.; Peng, Z. H.; Zhang, W. X.; Zhang, N.; Lai, W.; Zhang, Z. S.; Song, S.; Pan, D. S.; Ning, Z. Q.; Lu, X. P.; Zhang, X. W.; Zhang, C.; Li, J.; Xie, C. M.; He, Y.; Chen, L. Application of p21 and klf2 reporter gene assays to identify selective histone deacetylase inhibitors for cancer therapy. *Bioorg. Med. Chem. Lett.* **2011**, *21*, 110–116.
- (20) Zhao, H. Scaffold selection and scaffold hopping in lead generation: a medicinal chemistry perspective. *Drug Discovery Today* **2007**, *12*, 149–155.
- (21) Joucla, M.; Mortier, J. 2,5-Unsubstituted pyrrolidines from formaldehyde and amino acids through in situ azomethine-ylide 1,3-dipolar cycloaddition to alkenes. *J. Chem. Soc., Chem. Commun.* **1985**, *22*, 1566–1567.
- (22) Evans, D. A.; Mito, S.; Seidel, D. Scope and mechanism of enantioselective Michael additions of 1,3-dicarbonyl compounds to nitroalkenes catalyzed by nickel(II)-diamine complexes. *J. Am. Chem. Soc.* **2007**, *129*, 11583–11592.
- (23) Yan, L.; Budhu, R.; Huo, P.; Lynch, C. L.; Hale, J. J.; Mills, S. G.; Hajdu, R.; Keohane, C. A.; Rosenbach, M. J.; Milligan, J. A.; Shei, G. J.; Chrebet, G.; Bergstrom, J.; Card, D.; Mandala, S. M. 2-Aryl(pyrrolidin-4-yl)acetic acids are potent agonists of sphingosine-1-phosphate (S1P) receptors. *Bioorg. Med. Chem. Lett.* **2006**, *16*, 3564–3568.
- (24) For more information about HuPrime tumor-derived xenograft models versus traditional cell line-derived xenograft models, see the website of Crown Biosciences (Santa Clara, CA) at www.crownbio.com.
- (25) For more information, see www.ingenuity.com (Ingenuity Systems, Redwood City, CA).
- (26) See PubMed website: <http://methycancer.psych.ac.cn/MethyCancer.do>.
- (27) Cameron, E. E.; Bachman, K. E.; Myöhänen, S.; Herman, J. G.; Baylin, S. B. Synergy of demethylation and histone deacetylase inhibition in the re-expression of genes silenced in cancer. *Nat. Genet.* **1999**, *21*, 103–107.
- (28) Morris, M. R.; Gentle, D.; Abdulrahman, M.; Maina, E. N.; Gupta, K.; Banks, R. E.; Wiesener, M. S.; Kishida, T.; Yao, M.; Teh, B.; Latif, F.; Maher, E. R. Tumor suppressor activity and epigenetic inactivation of hepatocyte growth factor activator inhibitor type 2/SPINT2 in papillary and clear cell renal cell carcinoma. *Cancer Res.* **2005**, *65*, 4598–4606.
- (29) MacroModel, formerly known as BatchMin, is a general-purpose molecular mechanics program available from Schrödinger, L.L.C., New York. MacroModel was developed in the laboratories of Prof. Clark Still (Columbia University).
- (30) Friesner, R. A.; Murphy, R. B.; Repasky, M. P.; Frye, L. L.; Greenwood, J. R.; Halgren, T. A.; Sanschagrin, P. C.; Mainz, D. Extra precision Glide: Docking and scoring incorporating a model of

hydrophobic enclosure for protein–ligand complexes. *J. Med. Chem.* **2006**, *49*, 6177–6196.

(31) (a) Testino, S. A. J.; Patonay, G. High-throughput inhibition screening of major human cytochrome P450 enzymes using an in vitro cocktail and liquid chromatography-tandem mass spectrometry. *J. Pharm. Biomed. Anal.* **2003**, *30*, 1459–1467. (b) Walsky, R. L.; Obach, R. S. Validated assays for human cytochrome P450 activities. *Drug Metab. Dispos.* **2004**, *32*, 647–660. (c) Weaver, R.; Graham, K. S.; Beattie, I. G.; Riley, R. J. Cytochrome P450 inhibition using recombinant proteins and mass spectrometry/multiple reaction monitoring technology in a cassette incubation. *Drug Metab. Dispos.* **2003**, *31*, 955–966.

(32) Liang, G.; Guthrie, H. Automated electrophysiology in the preclinical evaluation of drugs for potential QT prolongation. *J. Pharmacol. Toxicol. Methods* **2005**, *52*, 123–135.